Improving spatial and temporal variation of ammonia emissions for the Netherlands using livestock housing information and a Sentinel-2-derived crop map

Xinrui Ge [a,b,*], Martijn Schaap [b], Wim de Vries [a,c]

[a] *Environmental Systems Analysis Group, Wageningen University, Wageningen, the Netherlands*
[b] *Department of Climate, Air and Sustainability, TNO, Utrecht, the Netherlands*
[c] *Wageningen Environmental Research, Wageningen, the Netherlands*

ABSTRACT

Ammonia emissions to the atmosphere have a range of negative impacts on environmental quality, human health, and biodiversity. Despite the considerable efforts in quantifying spatially explicit ammonia emissions, there are significant uncertainties in ammonia emission estimates at regional scales. We aimed to improve the modeling of atmospheric ammonia emission variability in space and time across the Netherlands by updating an agricultural ammonia emission model with a newly derived high-resolution crop map and a livestock housing location database of the Netherlands. To generate a crop map of 12 agricultural land cover classes, we applied random forest classification to the multi-temporal multispectral observations of surface reflectance and vegetation indices derived from Sentinel-2. The crop statistics were used to calculate ammonia emission distribution based on nitrogen demand (manure and mineral fertilizer needed) of different crop types using the INTEGRATOR model. Next, the crop map was utilized to spatially allocate the ammonia emissions to a high-resolution grid across the Netherlands. In addition, ammonia emissions from livestock housing systems were introduced as point sources using location data from the Geographic Information Agricultural Business system. The temporal emission variability was updated using a recently developed TIMELINES module. After the spatial and temporal distribution of ammonia emission was obtained with the crop map and housing information, it was imported into the chemistry transport model LOTOS-EUROS to model ammonia surface concentration for validation with in situ measurements.

The performed crop classification has an average accuracy score of 0.73. The derived crop map was compared with Dutch national statistics, and the results showed that the absolute median of the relative difference between Sentinel-2 derived crop areas and national statistical information is around 5%. The newly modeled ammonia monthly surface concentrations compared better with in situ measurements in terms of the magnitude and temporal variability than those derived from the original emission distribution, indicating that the temporal distribution of ammonia emissions was improved. The comparison of modeled and measured annual averaged surface concentrations illustrated that the spatial distribution of ammonia emission was also improved. All model performance indicators significantly improved, and the performance of the updated model was more stable and robust. The improvement was more evident at the stations where livestock housing is the main emission source. This study illustrates that apart from a satellite-derived crop map, information on the locations of animal housing systems also plays an essential role in better estimates of the spatial and temporal distribution of ammonia emissions. It can be worthwhile to extrapolate the method to other regions in Europe and elsewhere.

1. Introduction

Ammonia (NH$_3$) emission to the atmosphere has increased

substantially on a global scale during the twentieth century in response to the demand for food of a rapidly growing population that leads to enhanced nitrogen fertilization (Erisman et al., 2008). Large increases

---

* Corresponding author. Environmental Systems Analysis Group, Wageningen University, Wageningen, the Netherlands.
  E-mail address: jerry.ge@tno.nl (X. Ge).

are mainly witnessed in areas with intense agricultural activities, such as Europe, the US, and China, with declines in the last decade, especially in Europe (Schmitz et al., 2019) and the US (Gilliam et al., 2019) due to legislation. Ammonia is the primary form of reactive nitrogen in the environment (Sutton et al., 2014), and its primary emission source is agriculture which contributes to more than 90% of the total emissions in EU-28 (Elzing and Monteny, 1997; Velthof et al., 2012). Agricultural ammonia is lost to the environment during and after fertilizer and manure application to the land, through animal excretion in housing systems, and during grazing (Erisman et al., 2007; Galloway et al., 2003).

The atmospheric lifetime of ammonia is limited to several hours as it is effectively removed by dry and wet deposition (Fangmeier et al., 1994; Schaap et al., 2017). Once deposited, the reduced nitrogen components contribute to the acidification and eutrophication of forests and other (vulnerable) terrestrial ecosystems (Bowman et al., 2008, 2008de Vries et al., 2014), which can lead to biodiversity loss (Bobbink et al., 2010; Krupa, 2003; Midolo et al., 2019; van Dobben and de Vries, 2017). In addition, ammonia reacts with sulfuric and nitric acid in the atmosphere, leading to the formation of fine particulate matter (Schaap et al., 2004), which is an important cause of smog and consequently threatens human health with heart and lung conditions (Brunekreef and Holgate, 2002; Fowler et al., 2009; Pope et al., 2009). Ammonia remains a major concern as either near-zero or increasing trends have been observed in concentration and deposition measurements over large parts of Europe (Colette et al., 2016). Hence, a better understanding of ammonia emission and its fate in the atmosphere is of great significance.

The Netherlands is a densely populated, urbanized, and industrialized country in western Europe. As the second-largest exporter of food and agricultural products globally, the small country has a very intensive agricultural system (Dollmann et al., 2021). Consequently, the Netherlands has the highest ammonia emission density in Europe, with an average of about 3180 kg NH_3–N per square kilometer (Wever et al., 2019). Due to the short lifetime of ammonia in the atmosphere, a large fraction of the emission deposits within the country. It is modeled that Dutch agriculture contributes nearly half of the total nitrogen deposition to its nature areas (Stokstad, 2019). It is estimated that in 118 of 162 Dutch nature reserves, the nitrogen deposition exceeds critical load thresholds by an average of 50% (Stokstad, 2019). As control regulations have been gradually implemented in the last 30 years, the reported ammonia emissions in the Netherlands declined by 51% and 22% respectively between 1993 and 2005 and between 2005 and 2014, but the trends in emissions and concentrations of ammonia diverge over the period 2005–2014 (van Zanten et al., 2017). A recent study into this discrepancy showed that the effects of meteorological variability and changing atmospheric chemical regimes could explain one-third of the difference between the observed and modeled trends in concentrations (Wichink Kruit et al., 2017). The remaining inconsistency was not explained, but an incomplete understanding of the processes involved in ammonia emissions likely plays a crucial role in this context. However, because of expanding dairy operations, Dutch ammonia emissions have not significantly decreased in the last decade (Stokstad, 2019).

There are still significant uncertainties in ammonia emission estimates which are prone to considerable spatial and temporal variability (Battye et al., 2003; Erisman et al., 2007; Sutton et al., 2003, 2014). Many studies have highlighted that the spatial and temporal variability of ammonia concentrations modeled with chemistry transport models (CTMs) using static time profiles, such as GEOS-Chem (Bey et al., 2001; Paulot et al., 2014), MOZART-4 (Emmons et al., 2010; Liu et al., 2017), CHIMERE (Hamaoui-Laguel et al., 2011, 2014), LOTOS-EUROS (Hendriks et al., 2016), and PMCAMx (Pinder et al., 2006), is poorly represented and needs improvement. Several studies have developed approaches to include meteorology-dependent emission variability in CTMs (Backes et al., 2016; Hendriks et al., 2016; Skjøth et al., 2011). Many studies are based on the work of Ambelas Skjøth et al. (2004), who proposed a dynamic parameterization of the temporal variation of NH_3

emission based on meteorology, information about agricultural practice, and a simple crop growth model. The parameterization was then improved by including the effect of ventilation rates inside buildings, ambient wind speeds and a more realistic description of temperatures inside animal housing systems (Gyldenkærne et al., 2005). Werner et al. (2015) and Hendriks et al. (2016) showed that replacing the static emission profiles with those account for regional adaptation of meteorology and other variables improves the CTM performance against observations considerably.

At the same time, Ge et al. (2020) developed a novel ammonia emission model for Germany and the Benelux by combing an agricultural emission model (INTEGRATOR (de Vries et al., 2021; Kros et al., 2012)) and an agricultural management model (TIMELINES (Hutchings et al., 2012)). INTEGRATOR provided high-resolution (in the form of polygons called NCUs illustrated in Ge et al. (2020)) spatial distribution of ammonia emission, differentiating types of manure and fertilizer applied on croplands and grassland, grazing, and animal housing systems. TIMELINES (Hutchings et al., 2012) was adapted to provide the timing of manure and fertilizer application on various crops while housing emissions were prescribed following Gyldenkærne et al. (2005). The resulting spatially explicit crop type-, fertilizer type-, and animal housing type-dependent ammonia time profiles were used in the CTM LOTOS-EUROS (Manders et al., 2017). Although the evaluation against observations of ammonia showed a significant improvement, it was recognized that the spatial representation in the agricultural emission model, the so-called NCUs, which can be rather large areas, is a disadvantage. Within each NCU polygon, the emission is assumed to be evenly distributed, which does not reflect the distribution of crops and animal housing systems within the NCU. Hence, crop distributions and livestock housing information should be taken into account (Ge et al., 2020).

Many studies have used remote sensing data to perform analyses of vegetation indices time series to obtain agricultural land use and crop development information (Dubovyk et al., 2015; Marais Sicre et al., 2016; Vaglio Laurin et al., 2018; Waldhoff et al., 2017). The new Sentinel-2 instruments offer new opportunities to better distinguish between different crop types thanks to their sensor and orbit characteristics, high spatial resolution, and relatively short revisit time (Belgiu and Csillik, 2018; Kobayashi et al., 2020; Sonobe et al., 2018; Yi et al., 2020). Although new crop maps based on sentinel-2 are becoming available (Griffiths et al., 2019), their use for the quantification of agricultural ammonia emissions has not been explored yet.

This study aimed to improve upon the emission model of Ge et al. (2020) by introducing a high-resolution crop map and livestock housing information for the Netherlands. In this paper, we first describe the methodology of crop mapping from Sentinel-2 observations, the subsequent calculation of the spatial and temporal allocation of ammonia emission, which also accounts for livestock housing locations, and the evaluation of the updated emission product with the use of the CTM LOTOS-EUROS and in situ measurements. Next, we provide the results, including the obtained crop map, the updated emission estimates, and the validation of the emission products by comparing modeled surface concentrations with in situ measurements. Finally, we discuss the improvements in the emission model brought by the updated crop map and animal housing information and point out future perspectives for this work.

2. Methodology

The workflow in this study is separated into three steps (Fig. 1).

(1) Crop mapping through random forest classification using Sentinel-2 multi-temporal multispectral surface reflectance observations and vegetation indices calculated from surface reflectance.

(2) Adaptation of the spatial and temporal allocation of ammonia emissions by integration of the crop map and livestock housing
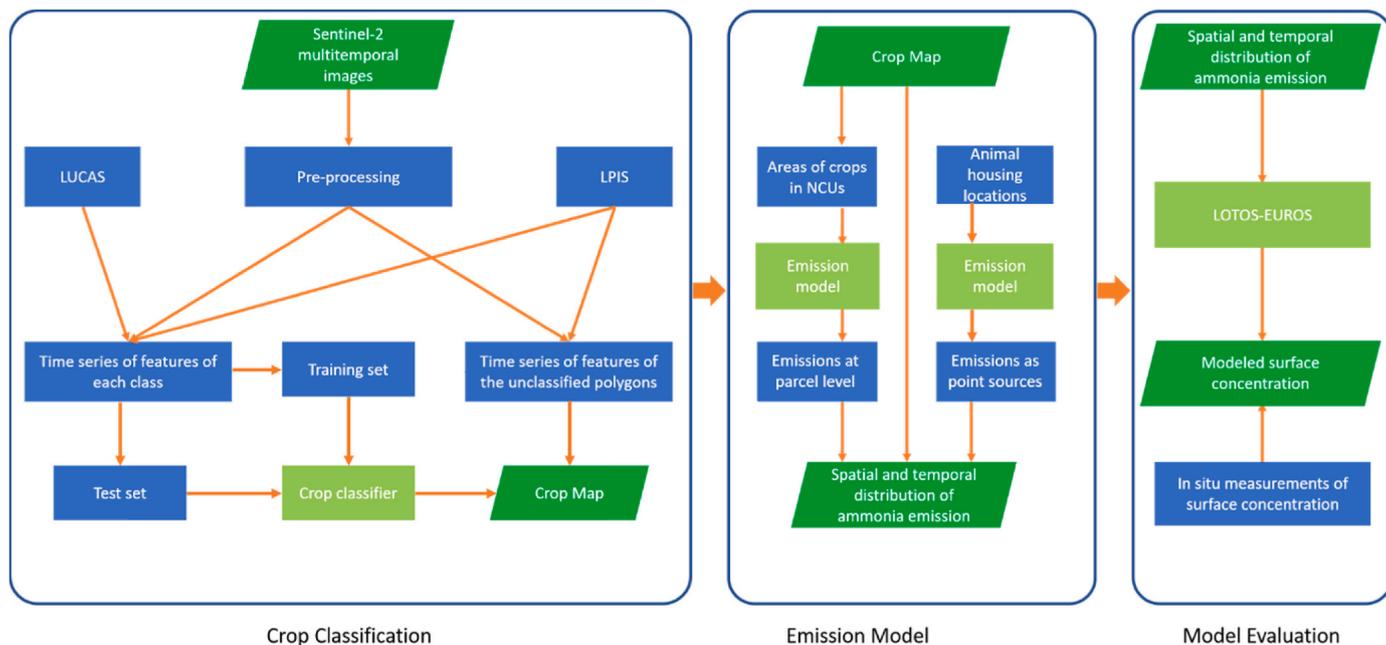
Fig. 1. The schematic workflow in this study is composed of three modules: crop classification that derives a high-resolution crop map of the Netherlands from Sentinel-2 observations, emission model that obtains the spatial and temporal distribution of ammonia emissions, and model evaluation with in situ measurements.

locations in the INTEGRATOR – TIMELINES emission model, described in Ge et al. (2020).

(3) Simulation of ammonia surface concentrations with the CTM LOTOS-EUROS using the original (without updates on crop map and livestock housing locations) and updated (with updates on crop map and livestock housing locations) ammonia emissions and validation of the simulated surface concentrations with in situ measurements.

Each of the steps is described in detail below.

2.1. Crop mapping with Sentinel-2 observations

Crop mapping is the process of identifying crop types and obtaining the spatial distribution of crops, which can be done with either conventional methods or automated machine learning-based methods. In a machine learning-based framework, crop types are determined using a crop classifier, which is an advanced tree-based, ensemble-based tool built by ground truth data to identify specific spectral and spatiotemporal crop signatures. Nowadays, multitemporal multispectral observations from optical satellites are used to estimate the spatial distribution of various crops due to their benefits of saving time and labor force (Yan et al., 2021). In this study, we conducted crop mapping by applying random forest classification to Sentinel-2 observations. An introduction to Sentinel-2 can be found in Section S.1 in the supplementary material, and random forest classification will be talked about in the text below. The study area for crop mapping covers not only the Netherlands but also North Rhine-Westphalia of Germany to increase the number of ground truth data. The area was divided into 263 patches of the sizes of 20,000 m by 20,000 m (see Fig. 2) for data downloading, pre-processing, processing and classification to save processing power and time.

The crop map of the Netherlands is obtained in the following steps.

(i) Collect ground truth land parcels from land surveys and georeferenced land parcels.

(ii) Derive the time series of Sentinel-2 surface reflectance and vegetation indices of the ground truth land parcels.
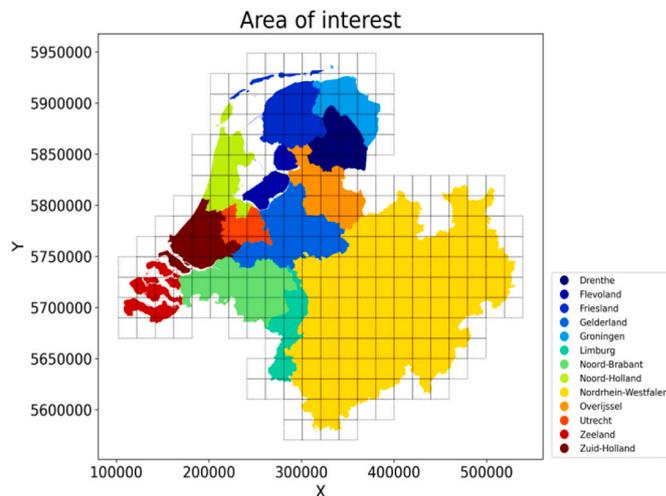
Fig. 2. The area of interest for crop mapping covers the Netherlands and North-Rhine Westphalia and is divided into 263 patches for data downloading and processing. The coordinates are in WGS84/UTM 32N coordinate system (EPSG:32,632).

(iii) Divide the ground truth land parcels into a training set and a test set. Obtain a crop classifier by applying random forest classification and determine the model performance by applying a 5-fold cross-validation.

(iv) Use the classifier to predict crop types for all land parcels, and assess the quality of the obtained crop map by comparing it with other statistical sources.

Details of the various steps are given in the sub-sections below.

2.1.1. Ground truth land parcels preparation

Eurostat has carried out the Land Use and Coverage Area frame Survey (LUCAS) every three years since 2006 to identify changes in the European Union in the socioeconomic use of land (for instance, agriculture) (Orgiazzi et al., 2018). LUCAS contains harmonized in situ land

cover and land use data collection based on observations made by surveyors throughout Europe (Ballin et al., 2018). The survey is conducted on a 2 km by 2 km grid, which means that land cover information is available at points that are 2 km away from each other. Since Sentinel-2 is available for full-year coverage from 2016 onwards, LUCAS 2018 data on arable crops and grasslands were selected in this study.

To reduce the uncertainties in Sentinel-2 observations and save processing time, we spatially averaged Sentinel-2 observations within each agricultural land parcel instead of looking at pixels. Land Parcel Identification System (LPIS) offers georeferenced polygons of agricultural plots derived from aerial photographs and high-precision satellite images (Montaghi et al., 2013; Zimmermann et al., 2016). The polygons demonstrate the exact shape and size of the land parcels whose contours often intersect with roads or other facilities. Therefore, we utilized QGIS to buffer each ground truth land parcel inwards by 10 m within its boundary so that tiny and narrow polygons were eliminated and the remaining polygons were ensured to lay within the farmlands or grassland. For each land parcel that contains a LUCAS point, we assigned the crop information to the land parcel to derive ground truth land parcels. We chose grassland and the 11 most common arable crops presented in the ground truth land parcels as the target classes. The arable crops are barley, flower, fodder, maize, nursery, oat, other cereal, potato, rye, sugar beet, and wheat.

2.1.2. Derivation of Sentinel-2 surface reflectance and vegetation indices time series

Satellite data from Sentinel-2 were downloaded through the open-source Python package *sentinelhub* (https://eo-learn.readthedocs.io/en/latest/) to access and process Sentinel-2 spatiotemporal satellite images. The Sentinel-2 observations used for crop mapping were Level 2A Bottom-Of-Atmosphere (BOA) reflectance. For specific days on which no Level 2A BOA reflectance data were available, we conducted pre-processing on Level 1C Top-Of-Atmosphere (TOA) orthoimages to create Level 2A BOA-corrected reflectance images, using the Sen2Cor processor (Main-Knorn et al., 2017). The pre-processing includes atmospheric, terrain, and cirrus correction (Li et al., 2018; Louis et al., 2016). Afterward, scene classification was conducted, resulting in a classification map of three classes of clouds and six other classes of shadows, cloud shadows, vegetation, not vegetated, water, and snow (Louis et al., 2010). Only pixels with less than 25% cloud probability were kept to ensure that all pixels used were under cloud-free conditions to reduce the impact of clouds. Besides, pixels in Sen2Cor's scene classification map labeled *NO DATA, Saturated or defective pixel, Cloud shadows, Cloud medium probability, Cloud high probability,* and *Thin cirrus* were regarded as invalid as well. When more than 60% of the pixels in an image were invalid, this image was removed.

In this study, 10-day averages of surface reflectance of 6 bands and 11 vegetation indices from February to November were utilized to derive their temporal patterns for machine learning. Most indices used were normalized differential indices based on differences in reflectance behavior between land cover types. For example, well-nourished, living plants absorb red light and reflect near-infrared light, while dead vegetation absorbs relatively less red light than healthy vegetation (Agapiou et al., 2014). Details on the chosen vegetation indices and their advantages are given in Section S.2 in the supplementary material. For each parcel, we calculated the time series of the spatially averaged surface reflectance and vegetation indices. Examples of the NDVI and EVI time series of the ground truth land parcels of grassland and maize are given in Section S.3 in the supplementary material.

It has to be noted that filtering was done to the ground truth parcels based on the 10-day averaged time series of surface reflectance to obtain more uniform ground truth data and to have a similar number of ground truth data for each crop type. When more than eight values were missing or invalid in a time series (30 values in total), the time series was left out. An outlier detection was performed on the observations to determine if an observation was invalid. For ground truth parcels of each crop type,

the mean (R_m) and standard deviation (R_{std}) of surface reflectance at each timestamp were calculated. The observations that lay outside $[R_m - cR_{std}, R_m + cR_{std}]$ were regarded invalid. The c is a constant that made sure there were no more than 30 valid time series for each crop.

2.1.3. Random forest classification

In this study, machine learning with random forest (RF) was used to obtain a crop classifier. The ground truth land parcels were divided into a training set (80%) and a test set (20%) using stratified sampling, which means that the samples were selected in the same proportion as they appeared in the original ground truth data. In this way, we eliminated the sampling bias in a test set and made sure that it represented the entire population. A 5-fold cross-validation was conducted to determine the robustness of the classifier. The ground truth data were divided into five batches, and RF machine learning was performed five times, with each time four batches (80%) being the training set and the remaining batch (20%) being the test set.

A random forest is a collection of a large number of individual decision trees on randomly selected samples (Breiman, 2001). By looking at features, a decision tree makes decisions by splitting nodes into sub-nodes to create relatively pure nodes. A feature, also known as a predictor variable, is an individual measurable property or characteristic used as input for effective algorithms in pattern recognition and classification (Bishop, 2016). This node-splitting process is performed multiple times during the training process until only homogenous nodes are left. Each decision tree returns a classification prediction, and the class with the most votes is the prediction of the forest (Lan et al., 2020). Compared to other algorithms, the random forest algorithm is considered more accurate and robust because of the enormous number of decision trees involved in the process (Guo et al., 2007). Taking the most voted class cancels out potential biases, which helps avoid the overfitting problem. Furthermore, when one set of observations does not have all feature values, RF can deal with the missing value, which is replaced with the median or the proximity-weighted average of all observations of that feature (Cutler et al., 2012). Last but not least, RF can diagnose the relative feature importance, which assists in selecting the most contributing features for classification (Rogers and Gunn, 2006). Variables with low importance might be omitted from the model, making it simpler and faster to fit and predict. RF has achieved efficient classification results in various remote sensing studies, including crop mapping (Hao et al., 2015; Novelli et al., 2016; Pelletier et al., 2016).

Regarding the random forest classification in this study, the 10-day averages of surface reflectance of 6 bands and 11 vegetation indices from February to November resulted in 510 features. The number of trees (ntree) should be chosen as large as possible, especially if the data comprises many predictors. The choice of ntree is usually a compromise between accuracy and computational speed (Janitza and Hornung, 2018). Goldstein et al. (2010) concluded that for their genome-wide data set, 1000 trees might be sufficient. Díaz-Uriarte and Alvarez de Andrés (2006) found that the results for random forests with 1000 trees and those for RF with 40,000 trees were almost the same. Genuer et al. (2008) found out that in the high-dimensional settings, RF with 500 trees yielded very similar out-of-bag (OOB) errors to that with 1000 trees. Following these findings and through experimentation, the number of trees was set to 1000 in this study. Following the random forest classification results reported by Belgiu and Drăguţ (2016) and Gislason et al. (2006), the number of variables used for tree nodes splitting (mtry) was established as the square root of the number of features and was set to 25.

After obtaining the crop classifier with the training set, we applied it to the test set and compared the predictions with the ground truth. The accuracy score of the classifier prediction on the test set, being the fraction of predictions our model succeeded in making, was 0.73. Fig. 3 shows the importance scores of the features and indicates that vegetation indices generally were given more weight than the Sentinel-2 bands, but there was no dominant feature, with importance values
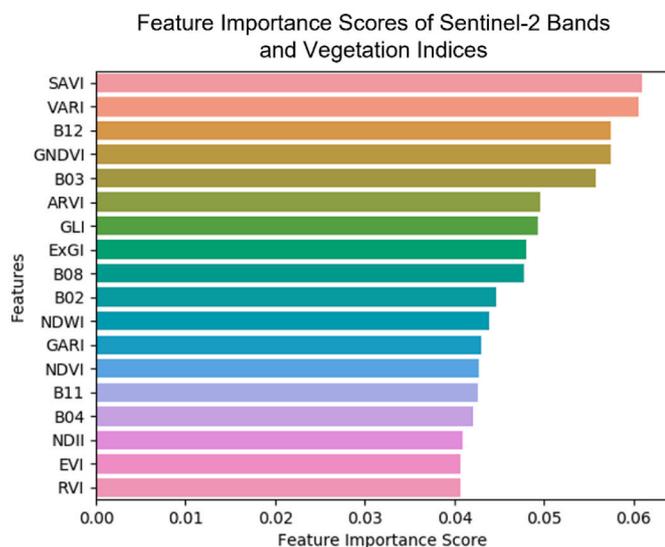
Fig. 3. Importance values of various feature values (6 satellite bands (B02, B03, B04, B08, B11, B12) and 11 vegetation indices shown in Table S1 in the supplementary material) used for machine learning.

ranging from 0.04 to 0.07. The accuracy scores of the 5-fold cross-validation were 0.67, 0.69, 0.69, 0.73, and 0.74 (0.71 on average), respectively. The resulting crop distributions are very similar. It means that the model was robust and not overfitted. As a result, we did not reduce the number of predictor features for crop mapping.

2.1.4. Derivation and validation of the crop map

After we calculated the same features (10-day averages of surface reflectance of 6 bands and 11 vegetation indices from February to November) of all crop parcels in the country in 2017, we applied the classifier to them to obtain a complete crop map of the Netherlands in 2017. Although the crop classifier was validated with the test data, it was important to verify the crop map on a national scale. Therefore, the resulting crop distribution was validated by comparing the predicted crop areas of grassland and the top four arable crops by area (maize, potato, wheat, and sugar beet) in each Dutch province with the official statistics in 2017 from Statistics Netherlands (CBS) (https://opendata.cbs.nl/#/CBS/en/dataset/7100eng/table). In addition, we also compared crop area per province to an online crop map dataset, OneSoil, to see how our map performed compared to a commercial service (https://map.onesoil.ai/).

2.2. Emission modeling with the updated crop map and housing information

As mentioned, the purpose of the study is to update the ammonia emission model described in Ge et al. (2020) with a detailed crop map and locations of animal housing systems. The emission model is composed of two modules, namely, a spatial allocator (INTEGRATOR) and a temporal allocator (TIMELINES) (Ge et al., 2020). The former generates the gridded annual emission map, while the latter disaggregates each gridded annual emission in time. INTEGRATOR is a static nitrogen cycling model which was used to calculate ammonia emissions from animal housing systems and manure and mineral fertilizer application (De Vries et al., 2020; Kros et al., 2012). For a detailed description of INTEGRATOR, we refer to De Vries et al. (2011) and Ge et al. (2020). For information on the temporal allocator TIMELINES, we refer to Ge et al. (2020). Below, we only describe the critical aspects of the approach to calculate the ammonia emissions from animal housing systems and manure and mineral fertilizer application. To account for the influence of emissions from outside the Netherlands, for example, by long-distance

transport, we chose the area of interest that covers the Netherlands and surrounding regions that may affect ammonia concentrations in the country. Therefore, being larger than the study area of crop mapping, the study area of ammonia emission modeling is $2°E-9°E$ in longitude and $50°N-54°N$ in latitude with a step of $0.015625°$ in longitude and $0.0078125°$ in latitude, resulting in a spatial resolution of approximately 1.7 km $\times$ 1.7 km.

In INTEGRATOR, the total N excreted was calculated by multiplying the number of animals at the NCU level with N excretion rates per animal per country for eight animal categories (dairy cows, other cows, pigs, laying hens, other poultry, sheep and goats, horses and fur animals). A division was made between the excretion of animals in housing systems and grazing animals in pastures based on national data for the number of grazing days. The N excreted in housing systems was derived by multiplying total N excretion with the housing fraction, while the N excreted on land during grazing was calculated by subtracting N excreted in housing systems from total N manure excretion. The total manure production was calculated from the N excreted in housing systems after correcting for losses (gaseous emissions and leaching) in housing systems.

2.2.1. Spatial distribution of annual emission from manure and fertilizer application using the crop map

Manure was distributed over grassland and arable crops using various allocation rules. Manure produced by grazing animals all entered grassland. Manure produced for sheep and goats was completely applied to grassland. For other manure, a fraction was applied to arable land, and the remaining fraction went to grassland/fodder crops, according to Menzi et al. (2002). Manure types were lumped into (i) liquid manure of dairy/other cattle, (ii) solid manure of dairy/other cattle, (iii) liquid manure of pigs, (iv) solid manure of pigs, and (v) poultry manure. Regarding fertilizer, a distinction was made between urea and other fertilizer. Manure distribution on arable land was divided over four arable crop groups, adapted after Velthof et al. (2009). The mineral fertilizer N demand of each crop was calculated by a balanced N fertilization approach based on the N demand of each crop (Ge et al., 2020). The ammonia emissions from grazing and application on arable crops and grassland were calculated by multiplying the N inputs by grazing cattle and by manure and fertilizer application with the corresponding N emission fractions.

The derived crop map influences the spatial distribution of ammonia emissions in two ways. First, the crop map leads to changes in manure distribution due to the above allocation rules and fertilizer distribution because of different nitrogen demands. Secondly, instead of evenly distributing emissions within the whole NCU as in Ge et al. (2020), we allocated the crop-dependent application emissions to where the corresponding crops are located within an NCU.

2.2.2. Spatial distribution of annual emission from animal housing systems using livestock housing information

The ammonia emissions from animal housing systems include emissions in animal houses and manure storage facilities. Ge et al. (2020) pointed out that allocating housing emissions evenly within each NCU was a source of uncertainties in the emission model. Therefore, animal housing locations are useful for treating housing emissions as point sources. Information on the locations of animal housing systems is based on the so-called GIAB (Geographic Information Agricultural Business) system, as used in the INITIATOR model, which is an adapted version of INTEGRATOR built specifically for the Netherlands (de Vries et al., 2015). GIAB includes information on the exact location of all housing systems of each farm in the Netherlands. (GIAB: (Gies et al., 2015); GIABplus (van Os et al., 2016):). Since we did not have direct access to GIAB, we used INITIATOR output for 2017, from which we extracted the coordinates of animal housing systems in the Netherlands. Then ammonia emissions from animal housing systems within each NCU were evenly assigned to the animal housing systems in that NCU as point

sources. The same animal categories in manure types were used in housing systems.

2.3. Surface concentration modeling for the evaluation with in situ measurements

To validate the improvement in the emission products brought by the crop map and livestock housing locations, we used the in situ measurements of surface concentrations in the Netherlands. The spatial and temporal distribution of ammonia emissions was imported into LOTOS-EUROS to calculate surface concentrations. LOTOS-EUROS is a 3-dimensional regional CTM (Manders et al., 2009, 2017; Schaap et al., 2008) that uses a description of the bidirectional surface-atmosphere exchange of ammonia (Wichink Kruit et al., 2017). The model is regularly used to address reactive nitrogen budgets (Banzhaf et al., 2015; Hendriks et al., 2016, 2016v; van der Graaf et al., 2018, 2020an der Graaf et al., 2020), and we refer to these publications for a detailed model description.

This paper conducted two LOTOS-EUROS simulation runs to quantify the changes in modeled ammonia concentrations brought by the update. The first base simulation (referred to as INT) used the INTE-GRATOR ammonia emission, which was distributed as described in Ge et al. (2020). The second (referred to as INT-SEN) utilized the emission information as described in the paper, using the updated crop distributions and livestock housing locations. For both simulations, non-agricultural emissions were derived from the TNO-MACC emission inventory (Kuenen et al., 2014).

Modeled ammonia surface concentrations were compared to in-situ measurements from the Measuring Ammonia in Nature (MAN) network. In this network, monthly mean ammonia concentrations at 255 sites in 60 Natura2000 areas were monitored (https://man.rivm.nl/) (Lolkema et al., 2015). Natura2000 areas have been designated to preserve the ecological value of natural areas, and they are protected under European legislation. The ammonia measurements from MAN use low-cost passive samplers. For the measurement method, calibration method, and uncertainties, we referred to Lolkema et al. (2015). When assessing the comparison of monthly and annual averaged concentrations, the stations were divided into three groups, which were determined by the primary source of local ammonia emission. If application emission or housing emission occupied more than 60% of the total emission within the grid where a station was located, this station was categorized as an application-dominated or housing-dominated station, respectively. The remaining stations were called "other stations". In this way, we could inspect the improvement brought by the updated crop map and animal housing systems information separately. In addition, measurements at all stations were also compared with the modeled results to assess the overall performance. The model performance indicators included relative bias, correlation, the normalized root mean square error (NRMSE), normalized mean absolute error (NMAE), model efficiency (EF), and index of agreement (IA) between the measurements and modeled results (see Ge et al. (2020) for the equations). In addition, the fraction of predictions that were within a factor of two of the observations (FAC2) were also calculated as it is a simple and robust measure, which is not overly influenced by the extreme values (high and low) in a time series. (Chang and Hanna, 2004; Hanna and Chang, 2012).

3. Results

3.1. The derived crop map

The national crop map derived from Sentinel-2 is presented in Fig. 4. The dominant agricultural land is grassland, with a total area near 1.0 million ha in the Netherlands, which is dominantly distributed in the provinces of Friesland (north), Overijssel (east), and Utrecht (center) (see Fig. 4(a)). Maize production is mainly found in the eastern part of the country (Drenthe, Eastern Overijssel, Eastern Gelderland, Nord-
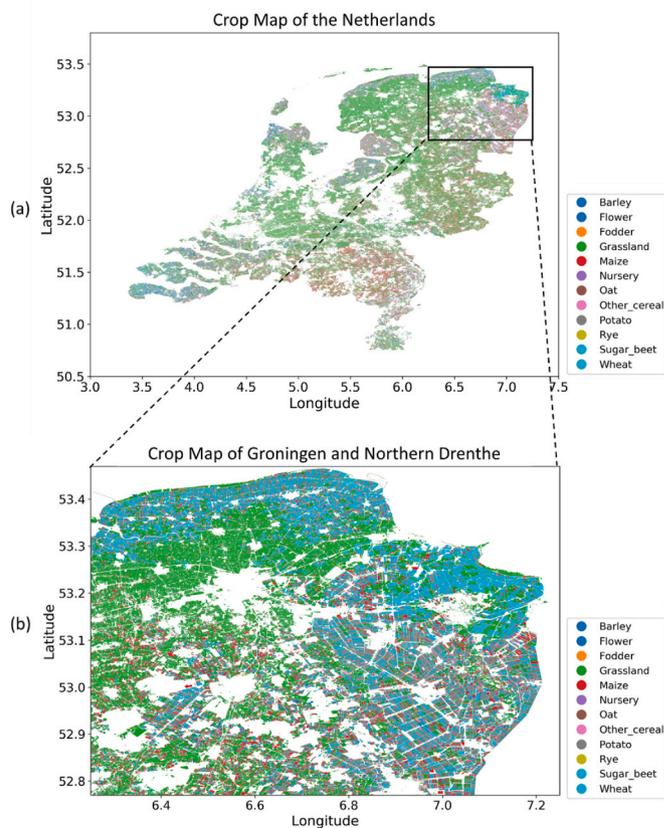

Fig. 4. Crop Map of the Netherlands (top) and the zoomed map of Groningen (bottom).

Brabant, and Limburg). As for potato, oat, wheat, and sugar beet, the distribution is less spread out but concentrated in some highly agriculturally active regions like Flevoland, the coastal areas of Friesland and Groningen, and along the German border in the north-east. Zeeland and Limburg in the south also have potato production but to a lesser extent. Regarding flowers, being a less important crop in terms of area, its fields are correctly identified in the provinces of Flevoland, North Holland, and some smaller areas like Noordwijkerhout and De Zilk. Fig. 4(b) shows the zoomed crop map of Groningen. One can see that grassland tends to be located in the lands inwards to the west, and arable crops (mainly wheat and potato) are mainly situated in the north by the ocean or to the east.

Based on the CBS dataset, important arable crops by area in the Netherlands are maize (218 k ha), potato (163 k ha), wheat (116 k ha), sugar beet (85 k ha), vegetables (61 k ha), and barley (30 k ha) (see Table 1). Table 1 summarizes the total areas of grassland and the six arable crops by area in the Netherlands, comparing estimates from our study with the Dutch statistics from CBS and with the statistics from the OneSoil. The crop areas derived from Sentinel-2 in our study demonstrate better alignment with CBS than those obtained from OneSoil for almost all crops except wheat and vegetables. The absolute median of the relative difference between Sentinel-2 derived crop areas and CBS is around 5%, while that between OneSoil and CBS is larger than 15%. The lowest deviations between the derived crop areas and CBS are found for grassland and barley, with the relative difference being −0.8% and 3.0%, respectively. However, the area of wheat obtained in this study is overestimated by 33%, while OneSoil has a lower relative error of 4.2%. Moreover, the obtained crop map rarely contains vegetables, while OneSoil also does poorly predict the vegetable area with a 60.7% deviation. We also compared the total area per province of grassland and the top four arable crops with the CBS statistics, and the details are given in Section S.4 in the supplementary material.

Table 1

Total production area for five major arable crops and grassland in the Netherlands (k ha) from Dutch statistics CBS, this study, and the OneSoil database, as well as the relative difference of the two estimates with respect to CBS data in 2017.

	Grassland	Maize	Potato	Wheat	Sugar beet	Vegetable	Barley
CBS	992	218	163	116	85	61	30
This study	984 (−0.8%)	207 (−5.1%)	171 (+4.9%)	155 (+33.0%)	103 (+20.7%)	0.01 (−100%)	31(+3.0%)
OneSoil	1139 (+14.8%)	258 (+18.5)	129 (−20.9%)	121 (+4.12%)	138 (+61.5%)	97 (+60.7%)	35 (+16.9%)

3.2. Ammonia emission distribution

Fig. 5 shows the original (left column, without the use of the crop map and livestock housing locations) and updated (right column, with updates on the crop map and livestock housing locations) annual ammonia emission maps in 2017. Fig. 5(a) and (e) show the national emission maps, whereas Fig. 5(b) and (f) are zoomed annual emission maps of Groningen. The updated maps are characterized by a high degree of granularity (spatial details) and a more prominent contrast in ammonia levels between agricultural and natural regions because the updated model only allocated emissions at sources instead of all over the NCUs, which eliminates ammonia emissions in non-agricultural areas. However, the main features of the ammonia emission distribution across the country are comparable to the original data. Cattle housing
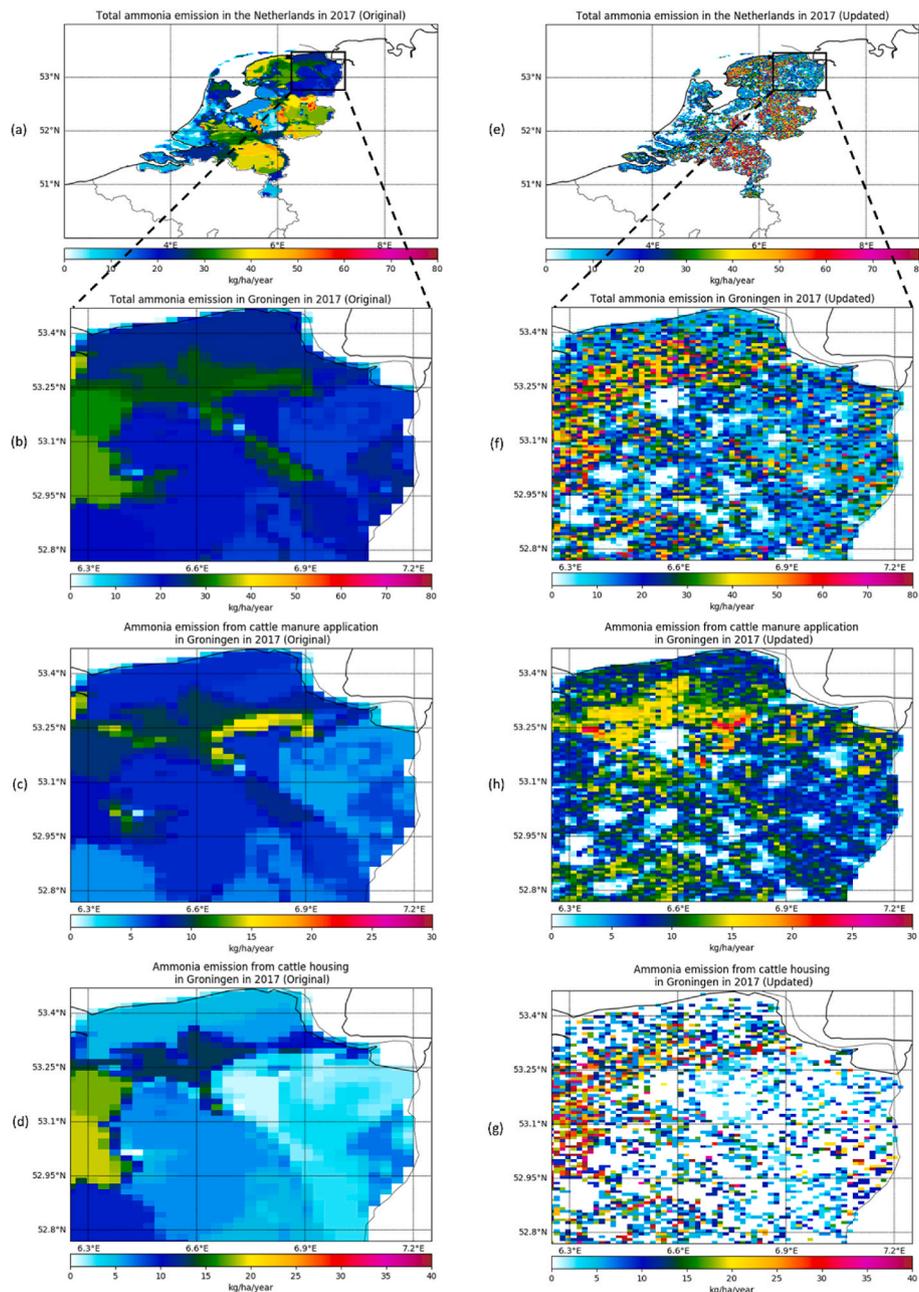
Fig. 5. Maps of the spatial variation (presented at 1.7 km × 1.7 km resolution) in annual total ammonia emission over the Netherlands (a, e), and zoomed map of total emission (b, f), cattle manure application emission (c, g) and cattle housing emission (d, h) in Groningen.

emissions in Fig. 5(h) are point sources, so they are less spread out and at larger magnitudes than in Fig. 5(d). Significant differences in spatial distribution also occur from cattle manure application (Fig. 5(c) and (g)). For example, the application emission level in Fig. 5(c) is much higher in the north, close to the coast, and other new hot spots appear in central Groningen because the derived crop map affects the spatial allocation of ammonia emissions and introduces new maxima in the distribution. The crop map tells that northern Groningen is mainly occupied by potatoes and wheat. However, the original land use input data of INTEGRATOR indicate that there is broader coverage for vegetables than potatoes in this area. INTEGRATOR regards potato as an arable crop with intermediate manure use, whereas it does not allocate manure to vegetables, which results in more manure allocated here in the updated model. Furthermore, since different crops have different timings of fertilization (Ge et al., 2020), the temporal distribution of the gridded emissions is also affected, causing emission peak shifts over the year. To summarize, the accuracy of the crop distribution in the emission model is significant in estimating manure/fertilizer distribution and the subsequent spatial and temporal distribution of ammonia emission.

3.3. Comparison of the modeled and measured ammonia surface concentrations

3.3.1. Monthly averaged ammonia surface concentrations

Fig. 6 shows two examples comparing ammonia surface concentrations measured in the MAN network and simulated with the original and updated emission products. In both Fig. 6(a) and (b), the updated modeled result shows better correspondence with the measured concentrations, both in absolute magnitude and temporal variability. Both INT and INT-SEN simulations show the spring and autumn peaks of surface ammonia concentration at the application-dominated Station Lauwersmeer-De Middelplaat (Fig. 6(a)). However, the spring peak predicted by the INT scenario is largely overestimated, while INT-SEN simulated the time series more accurately. Regarding the housing-dominated Station Sarsven en De Banen- Sarsven (Fig. 6(b)), the modeled temporal variabilities in both simulations are relatively similar,

except that the average concentration in the updated INT-SEN simulation is higher than that from the INT simulation and better aligned with the measurement. The INT simulation shows an earlier spring peak than the measurements. This is because the original model distributes housing emissions to the whole NCU, which smoothens spatial characteristics and reduces ammonia levels in the grid cell. In contrast, the updated model keeps housing emissions where animal housing systems are located, leading to higher ammonia levels in the grid cell.

Fig. 7 shows the scatter plots comparing modeled and measured monthly averaged surface concentrations at application-dominated stations (Fig. 7(a) and (b)), housing-dominated stations (Fig. 7(c) and (d)), other stations (Fig. 7(e) and (f)) and all stations (Fig. 7(g) and (h)). Table 2 presents the model performance indicators for the comparison of simulated and measured monthly averaged surface concentrations in the INT and INT-SEN simulations for the four groups of stations. At application-dominated stations, both simulations seem to over-allocate a considerable amount of emission in springtime (February, March, and April) to account for the fertilization of spring crops. The overestimation in spring in the INT-SEN simulation is less severe, and the spread of the scatter points is narrower (Fig. 7(b)), resulting in better model performance indicators (see Table 2). Similar results are observed in the comparison at other stations. In Fig. 7(c) and (d), there is both under- and overestimation for both comparisons in springtime, with the updated model reducing the deviations compared to the original model. However, for summer, the majority of the scatter points are still located above the y = x line, which means that the tendency to overestimate the ammonia levels in summer remains. At housing-dominated stations, the improvement is more evident, even though the overestimation in summer remains. In Table 2, almost all indicators have improved except that the bias for housing-dominated stations remained almost the same (slight increase). Error measures, including relative standard deviation, NRMSE, and NMAE, have dropped substantially, especially for housing-dominated stations. The reductions in relative standard deviation and NMAE are more pronounced than those in the NRMSE. This is because the individual differences are weighted equally in the standard deviation and NMAE calculation, while the NRMSE gives a relatively high weight
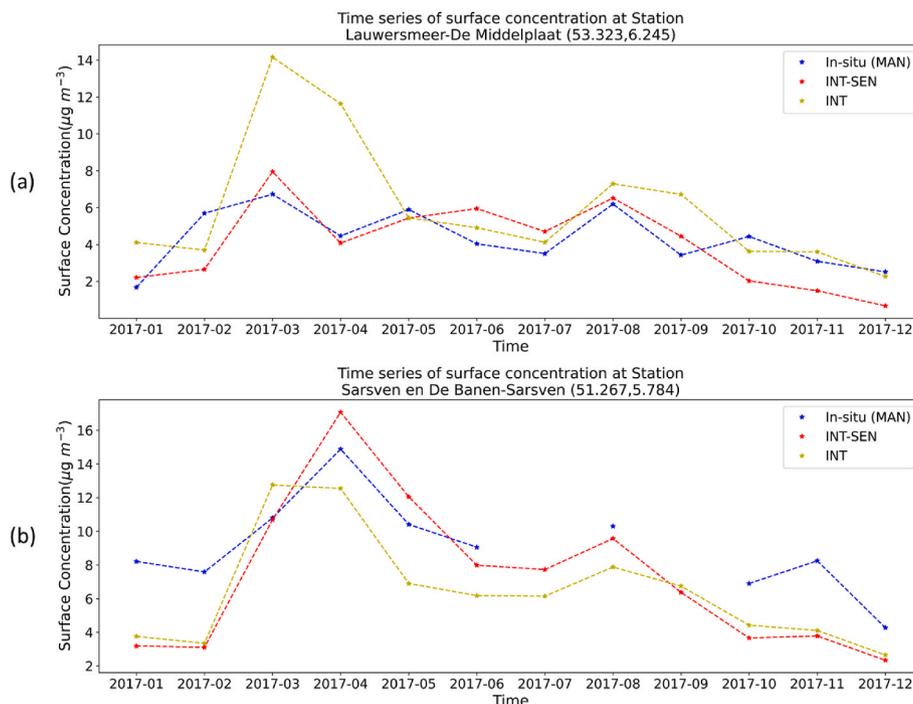

Fig. 6. Comparison of surface ammonia concentration time series measured in the MAN network and modeled with the original emissions (the INT simulation) and the updated emissions (the INT-SEN simulation) at an application-dominated station (top) and a housing-dominated station (bottom). There were no valid data for July and September.
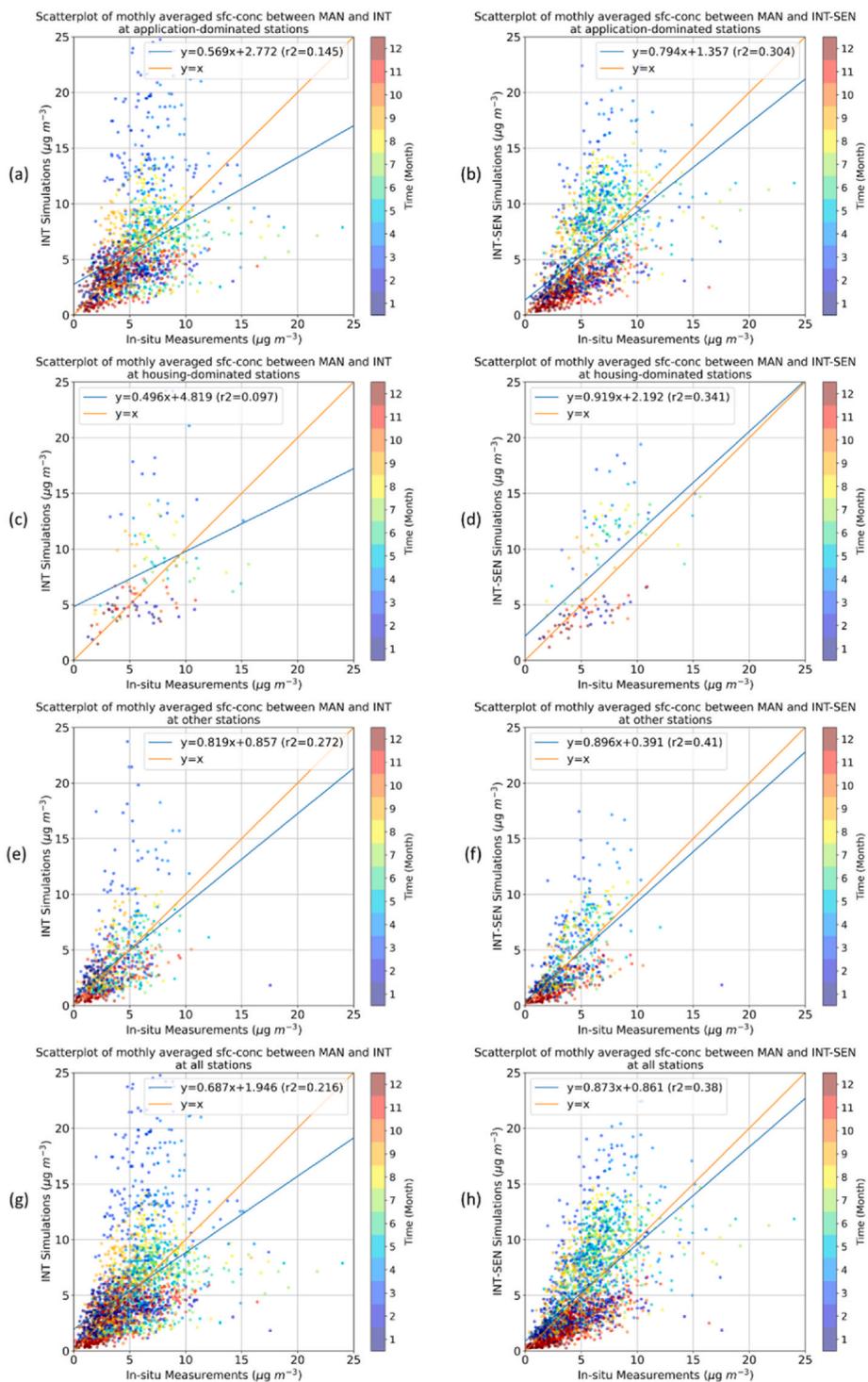
Fig. 7. Scatter plots of monthly averaged modeled and measured ammonia surface concentrations comparing the original (the left panel) and updated (the right panel) modeled results with measurements at application-dominated stations (a, b), housing-dominated stations (c, d), other stations (e, f) and all stations (g, h).

to large errors (overestimation in spring). In addition, both model efficiency and index of agreement suggest that the INT-SEN simulation can reproduce and predict ammonia surface concentrations in better agreement with in situ measurement. Finally, the FAC2 factors of INT-SEN modeled results are larger than those of INT simulations for any station type, which means that the INT-SEN model is more robust and less influenced by extreme values.

3.3.2. Annual averaged ammonia surface concentrations

Annual averaged ammonia surface concentrations were also calculated, giving insight into the quality of the spatial distribution of estimated ammonia emissions. Fig. 8 shows the scatter plots of comparisons between measurements and the two simulations INT and INT-SEN at application-dominated stations, housing-dominated stations, other stations, and all stations. Table 3 summarizes model performance indicators for the comparison. At application-dominated stations (Fig. 8 (a) and (b)), all indicators have been improved (see Table 3), with scatter points being much more concentrically distributed around the y = x line and narrower width of spreading, which corresponds to a higher correlation and lower errors. For housing-dominated stations (Fig. 8(c)

Table 2

Quality assessment of the comparison between measured monthly averaged surface concentrations and simulated concentrations with the original (INT) and updated (INT-SEN) INTEGRATOR model.

Station type	Simulation	Rel. bias (%)	Rel. std (%)	Correlation	NRMSE	NMAE	EF	IA	FAC2
Application -dominated	INT	6.68	72	0.38	14	45	0.05	0.57	0.75
	INT-SEN	0.53	56	0.55	13	40	0.28	0.71	0.76
Housing-dominated	INT	22.02	69	0.31	20	41	0.04	0.53	0.78
	INT-SEN	22.13	50	0.58	20	33	0.22	0.70	0.84
Other	INT	6.00	80	0.52	12	49	0.25	0.67	0.68
	INT-SEN	3.77	60	0.64	12	44	0.40	0.77	0.74
All	INT	7.58	74	0.46	13	46	0.16	0.64	0.73
	INT-SEN	1.06	58	0.62	12	40	0.29	0.75	0.76

and (d)), all indicators except relative bias have been improved (see also Table 3). The most remarkable improvement is the increased correlation between observations and predictions at housing-dominated stations (from almost 0 to 0.45) since housing emissions are point sources in the updated model. When looking at all stations (Fig. 8(g) and (h)), we can conclude that the spatial distribution of ammonia emission has been improved.

4. Discussion

This paper aimed to improve the spatial and temporal distribution of ammonia emission estimates by updating the agricultural emission model INTEGRATOR with a high-resolution crop map obtained with Sentinel-2 observations and livestock housing information. Their impact on the spatial distribution of manure distribution and N excreted in housing resulted in higher details of ammonia emissions in space and time. Evaluation of the measured and modeled ammonia surface concentration data illustrated that the model improved the spatial and temporal emission estimates, although certain divergences between modeled and observed concentrations remain. Below, we discuss the main directions for improvement based on this work.

4.1. Crop mapping

The acquisition of ground truth data plays a major part in developing and validating land cover maps (Foody et al., 2016; Kavzoglu, 2009). This study employed the LUCAS database as the ground truth for machine learning, being one of the most extensive training samples for large-scale crop mapping in Europe. However, there exist some challenges. First of all, geolocation errors related to GPS measurements in the field and image misregistration errors contribute to wrongly classified ground truth data, resulting in a miscalculation of the temporal variability of vegetation indices of the training samples and test samples (Mack et al., 2017). Secondly, LUCAS georeferenced observation points are aligned on a 2 km by 2 km grid, which means that the number of data points for certain crop classes might be too limited. For a selected area, regardless of the size, there may be limited availability of training data for less-grown crops but an abundant number of samples for the most common crop types. For instance, the number of training samples is only five for vegetables compared to more than dozens for other crops and grassland. It is a known challenge to map small-sized classes and estimate the associated accuracy (Stehman, 2000), as larger classes significantly impact overall accuracy. Furthermore, dominant land cover classes in the training data are classified at the expense of smaller classes because the overrepresentation of larger classes in a land cover map mainly affects the validation results of the smaller class. We observed such effects, for example, between wheat, the larger class, and vegetables, the smaller class. Even though vegetables should cover various plants with different temporal patterns in vegetation indices, the training sample of vegetables in this study showed spectral similarities with wheat in the training data. This is why vegetables rarely appeared in our crop map and wheat cover was overestimated.

The spectral properties of a target class and the size of crop parcels also play an essential role in crop mapping. From the extensive validation with the CBS dataset and comparison to the OneSoil database, it can be seen that good validation results were achieved for maize and grassland (see Table 1 and Fig. S2 in the supplementary material), which have relatively distinct temporal patterns of reflectance and vegetation indices (see Fig. S1 in the supplementary material). On the contrary, cereal types, including rye, wheat, and oat, have similar phenological and morphological patterns, hampering their spectral differentiation and resulting in lower classification accuracy for the classes. Moreover, smaller parcel sizes may also have affected classification accuracy as the risk of mixing spectral properties with adjacent land covers increases. This hinders the compilation of representative training data and subsequent land cover predictions.

The misclassification in crop types impacts ammonia emission estimates in INTEGRATOR because different arable crop groups have different manure demands. The impact is limited for the cereal types (rye, wheat, and oat) since they are all in the same group of intermediate manure use. However, for instance, when vegetables are classified as wheat, an overestimation in ammonia application emission will occur because no manure is applied to vegetables. In contrast, wheat belongs to the crop group with intermediate manure use.

To further improve classification accuracy, collecting additional training data through manual or automated approaches may help to distinguish spectrally or temporally distinct classes (Radoux et al., 2014). Besides additional ground truth data, integrating other multi-sensor time series such as Landsat-7, Landsat-8, and MODIS, which provides observations of similar nature as Sentinel-2, allows improving the temporal frequency of time series, shortening the revisit time to 2–5 days (Drusch et al., 2012; Wulder et al., 2015). Finally, there have been studies exploring the synergies of optical and high-resolution synthetic aperture radar (SAR) time series (e.g., from Sentinel-1 C-Band) for the mapping and analysis of phenology in agricultural land cover (Baumann et al., 2018; Mercier et al., 2019; Reiche et al., 2018). Unlike optical images, whose quality and availability may be affected by the presence of clouds and haze, SAR sensors can gather data regardless of weather conditions and sun illumination, resulting in a more frequent revisit time (Clerici et al., 2017; Mestre-Quereda et al., 2020). These techniques may be used to discriminate crop types better in the future.

4.2. Emission model assessment

After the comparison with MAN in situ measurements, one can see that the updated emission model has improved both the spatial (Table 3) and temporal (Table 2) distribution of ammonia emission, while the improvement is more evident at housing-dominated stations.

The model simulations at the application-dominated stations (Fig. 7 (a) and (b)) showed an overestimation of ammonia surface concentration in springtime (February, March, and April). However, it is less severe when using the improved emission product. There are three possible explanations. First and foremost, it could be incorrect crop information, which leads to inaccurate manure and fertilizer distribution that affects the spatial distribution, and estimated fertilization day that impacts the temporal distribution of ammonia emissions. In the original
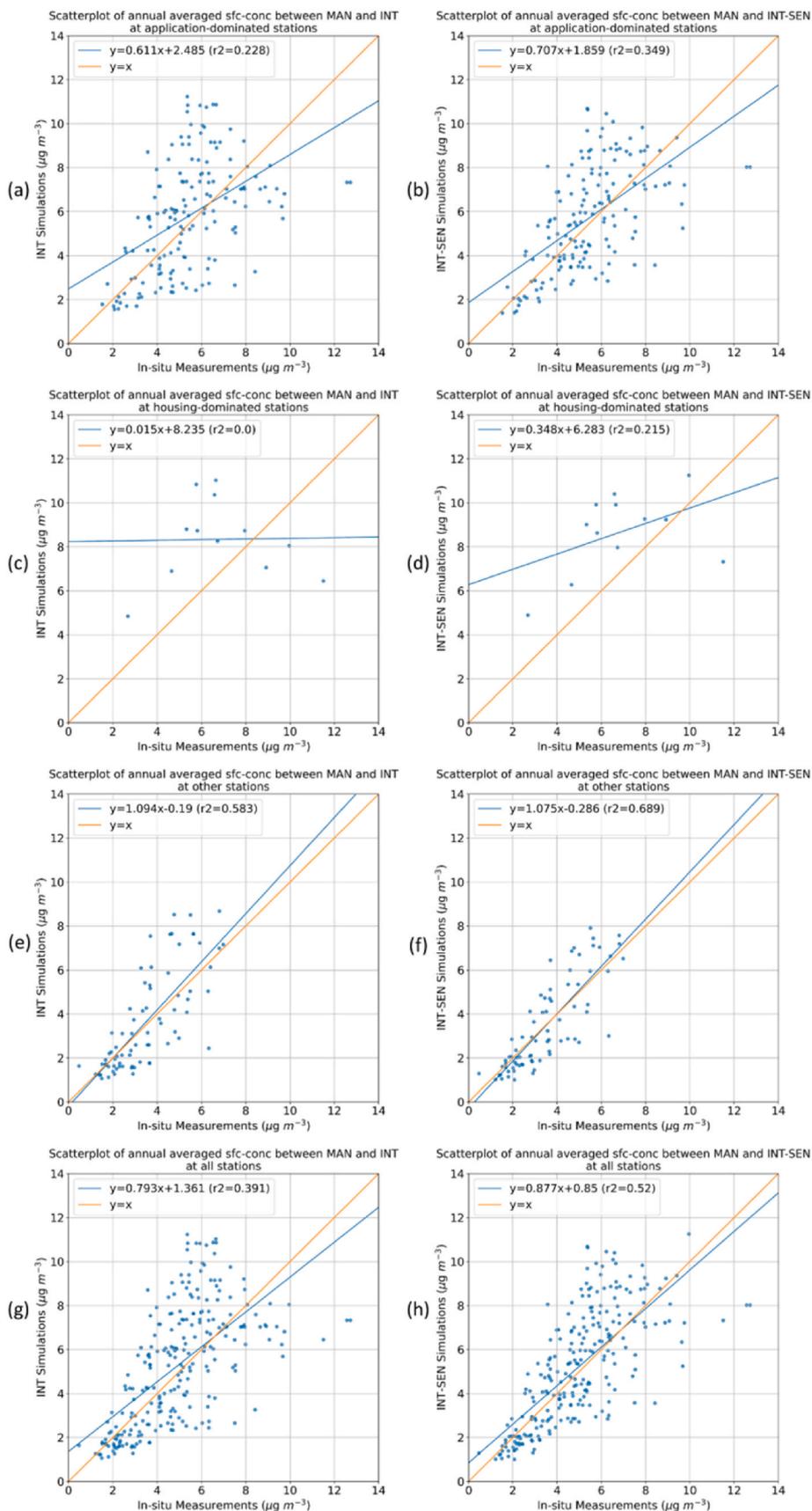
Fig. 8. Scatterplot plot of annual averaged ammonia surface concentrations comparing the original INT (the left panel) and updated INT-SEN (the right panel) simulated results with measurements at application-dominated stations (a, b), housing-dominated stations (c, d), other stations (e, f) and all stations (g, h).

Table 3

Quality assessment of the comparison between measured annual averaged surface concentrations and simulated concentrations with the original (INT) and updated (INT-SEN) INTEGRATOR model.

Station type	Simulation	Rel. bias (%)	Rel. std (%)	Correlation	NRMSE	NMAE	EF	IA	FAC2
Application-dominated	INT	6.61	43	0.48	24	32	0.11	0.67	0.93
	INT-SEN	1.02	35	0.59	21	27	0.28	0.76	0.97
Housing-dominated	INT	21.22	42	0.02	52	35	−2.32	0.45	1
	INT-SEN	22.07	32	0.45	43	27	−1.41	0.63	1
Other	INT	3.90	42	0.76	19	31	0.57	0.84	0.92
	INT-SEN	5.76	32	0.83	16	27	0.68	0.89	0.93
All	INT	7.03	44	0.62	21	32	0.35	0.77	0.93
	INT-SEN	0.99	36	0.72	17	27	0.51	0.84	0.96

emission model, due to outdated land use data in INTEGRATOR and an allocation algorithm distributing emissions from fertilization evenly within each NCU, the derived emission maps are smeared out, even including relatively strong emissions from non-agricultural areas. In the updated model, crops sown and fertilized between spring and autumn can be wrongly classified as spring crops. As a result, emissions that are supposed to occur in late spring are allocated to early spring. Secondly, the emission fractions used to derive ammonia emission from applied nitrogen could be inaccurate. Even though emission fractions influence annual total emissions, more emissions are allocated at peaks than at other times in a year during temporal allocation, leading to larger uncertainties at peaks. The emission fractions in INTEGRATOR are country-dependent constants that only differentiate among manure and fertilizer types. They neglect the influence of meteorological conditions, soil properties, application methods, etc. For example, air temperature has a positive impact on ammonia volatilization (Sommer et al., 1991). When the realistic temperature during fertilization in the Netherlands is lower than the assumed average temperature used to estimate emission fractions in INTEGRATOR, annual application emission totals and spring emissions will be overestimated. The last possible source of overestimation in spring is the misrepresentation of ground station measurement in the simulations. The MAN stations can be seen as points, so the distance between a station and the emission source plays an essential role in the measured values. If a station within a grid cell is located close to a farm, then the effect of overallocation to spring will be strengthened due to higher sensitivity. Even though the spatial resolution of the two model runs is 1.7 km × 1.7 km, it cannot fully represent what a ground station measures.

At housing-dominated stations, the comparison of surface concentrations has low correlations (see Table 2), and the spread in the scatter plots is quite wide (Fig. 7(c) and (d)). The updated modeled results have improved, but there still exist considerable errors. Firstly, even though housing emissions are treated as point sources and assigned to where animal housing systems are located, housing emissions are still evenly divided among animal housing systems in one NCU, regardless of the differences in animal numbers and N excretion in the houses due to the lack of data availability. This brings out the errors in the absolute ammonia emission level at individual locations. Secondly, there is still an overestimation in March/April because housing-dominated stations are still affected by the uncertainties of application emissions. Last, the difference in modeled and measured ammonia surface concentrations also comes from the uncertainties of the MAN measurements, including the random uncertainties of a single MAN measurement, the calibration procedure, and the calibration standard (Lolkema et al., 2015). The relative uncertainty decreases with the magnitude of the ammonia concentration, from 41% to 20% when measured monthly average ammonia concentrations increase from 1 to 20 $\mu g \cdot m^{-3}$ (Lolkema et al., 2015).

Other systematic errors also affect the uncertainty and inaccuracy in the spatial and temporal allocation of ammonia emissions, such as the negligence of alternative emission sources and the spatial variability of emission fractions. For example, animal waste like manure not only goes to storage facilities but also is handled in biogas powerplants, which was

not accounted for in the study and will have affected the spatial distribution of ammonia emission depending on biogas powerplant locations. Additionally, the spatial variation of housing type for each animal category in each country was not taken into account. The emission fractions for animal houses and manure storage in INTEGRATOR are a function of animal category and manure category (solid manure or liquid manure) per country (De Vries et al., 2020; Kros et al., 2012). The differences in countries are related to the animal houses and manure storage facilities that occur (high, medium, or low emission systems). One average housing or storage type per country and animal category is used without distinguishing the differences within a country. Describing the fraction of excreted nitrogen that volatilizes as ammonia as a constant may cause large uncertainties in local scale estimations. Ammonia emissions from animal excretion are highly climate-sensitive (Jiang et al., 2021). Sutton et al. (2013) showed an increase in emission rates of a factor of nine between 5 and 25 °C, with additional effects from humidity and precipitation (Riddick et al., 2017). Skjøth and Geels (2013) emphasized the substantial impact of annual variations in meteorology and variations in overall climate on ammonia emissions because the volatilization of ammonia is very sensitive to air temperature. They argued that emissions could easily vary by 20% for different geographical locations within a country due to overall variations in climate. The amount of nitrogen emitted as ammonia from manure application is also affected by soil properties, such as soil pH, soil moisture, and mineral soil substrate (Raymond et al., 2016). The soil pH can significantly affect ammonia volatilization positively, meaning higher soil-pH values lead to higher rates of ammonia volatilization (Raymond, 2016). There are spatial variations in the geographical distribution of soil pH, and the typical values range between 5.8 and 7.0 depending on the crop types, which is usually lower than the pH of manure (Riddick et al., 2016).

There is limited research on determining the magnitude of ammonia emissions from farming while considering the effects mentioned above. Most of the previous studies used empirical methods. For instance, Sommer and Hutchings (2001) reviewed various empirical models that used experiment-derived equations to predict ammonia volatilization from slurry application. However, only one or two factors were studied, and the interactions between these factors were not investigated. Misselbrook et al. (2000) derived ammonia emission fractions under various farming practices in the UK, but the impacts from climate are only accounted for to a small extent in these emission factors. Another method for estimating ammonia emission fractions is to use process-based models, which take into account a theoretical understanding of relevant processes (Móring et al., 2016; Nemitz et al., 2001; Sutton et al., 1995). For field-applied slurry, Hafner et al. (2019) built a semi-empirical dynamic model to predict ammonia volatilization as well as emission fractions. Values for parameters that quantify the effects of the following predictor variables on partitioning and transfer rates were estimated: slurry dry matter, application method, application rate, incorporation (shallow or deep), air temperature, wind speed, and rainfall rate. Moreover, along with ammonia emission, soil pH changes simultaneously because the hydrolysis of ammonia production can change the soil pH. Móring et al. (2016) proposed a dynamic scheme for

simulating soil pH in a field scale model and had a reasonable approximation against measurement. We think that detailing the emission fraction dynamically could be a worthwhile step to improve the emission model further.

5. Conclusions

A Sentinel-2-derived high-resolution crop map and the locations of animal housing systems in the Netherlands were used to update an ammonia emission model, resulting in more refined spatial details and temporal variability of ammonia emissions across the country. Using the crop map and housing information in LOTOS-EUROS, the modeled monthly and annual ammonia surface concentrations compared better with in situ measurements than those derived with the original emission product, indicating that the spatial and temporal distribution of ammonia emission estimates was improved. The model captured the magnitude and temporal variability of in situ measurements at both application-dominated and housing-dominated stations. Almost all model performance indicators have improved, with more significant improvements at housing-dominated stations. However, the model still had uncertainties, illustrated by the overestimated ammonia emission in spring. The findings indicate that including the locations of livestock housing systems and the satellite-derived crop map has improved ammonia emission estimates in space and time, and the methodology can be relatively easily applied to a larger region such as EU-27. The next step to refine the emission model would be replacing the constant emission fractions of animal housing and manure/fertilizer application with spatially explicit ones that account for the spatial variations in explanatory variables related to meteorology, manure properties, application method, and soil properties.

Code availability

LOTOS-EUROS is available for download under license at https://lotos-euros.tno.nl/.

CRediT authorship contribution statement

Xinrui Ge: Conceptualization, Methodology, Software, Validation, Visualization, Investigation, Writing – original draft. **Martijn Schaap:** Supervision, Writing – review & editing. **Wim de Vries:** Supervision, Writing – review & editing.

Declaration of competing interest

The authors declare that they have no known competing financial interests or personal relationships that could have appeared to influence the work reported in this paper.

Data availability

Data will be made available on request.

Acknowledgments

Appendix A. Supplementary data

Supplementary data to this article can be found online at https://doi.org/10.1016/j.aeaoa.2023.100207.

References

Agapiou, A., Alexakis, D.D., Sarris, A., Hadjimitsis, D.G., 2014. Evaluating the potentials of sentinel-2 for archaeological perspective. Rem. Sens. 6, 2176–2194. https://doi.org/10.3390/rs6032176.

Ambelas Skjøth, C., Hertel, O., Gyldenkaerne, S., Ellermann, T., 2004. Implementing a dynamical ammonia emission parameterization in the large-scale air pollution model ACDEP. J. Geophys. Res. Atmos. 109 https://doi.org/10.1029/2003JD003895.

Backes, A., Aulinger, A., Bieser, J., Matthias, V., Quante, M., 2016. Ammonia emissions in Europe, part I: development of a dynamical ammonia emission inventory. Atmos. Environ. 131, 55–66. https://doi.org/10.1016/j.atmosenv.2016.01.041.

Ballin, M., Barcaroli, G., Masselli, M., Scarnó, M., 2018. Redesign Sample for Land Use/ Cover Area Frame Survey (LUCAS) 2018. Eurostat. https://doi.org/10.2785/132365.

Banzhaf, S., Schaap, M., Kranenburg, R., Manders, A.M.M., Segers, A.J., Visschedijk, A.J. H., Van Der Gon, H.A.C.D., Kuenen, J.J.P., Van Meijgaard, E., Van Ulft, L.H., Cofala, J., Builtjes, P.J.H., 2015. Dynamic model evaluation for secondary inorganic aerosol and its precursors over Europe between 1990 and 2009. Geosci. Model Dev. (GMD) 8, 1047–1070. https://doi.org/10.5194/gmd-8-1047-2015.

Battye, W., Aneja, V.P., Roelle, P.A., 2003. Evaluation and improvement of ammonia emissions inventories. Atmos. Environ. https://doi.org/10.1016/S1352-2310(03)00343-1.

Baumann, M., Levers, C., Macchi, L., Bluhm, H., Waske, B., Gasparri, N.I., Kuemmerle, T., 2018. Mapping continuous fields of tree and shrub cover across the Gran Chaco using Landsat 8 and Sentinel-1 data. Remote Sens. Environ. 216, 201–211. https://doi.org/10.1016/j.rse.2018.06.044.

Belgiu, M., Csillik, O., 2018. Sentinel-2 cropland mapping using pixel-based and object-based time-weighted dynamic time warping analysis. Remote Sens. Environ. https://doi.org/10.1016/j.rse.2017.10.005.

Belgiu, M., Drăguţ, L., 2016. Random forest in remote sensing: a review of applications and future directions. ISPRS J. Photogrammetry Remote Sens. 114, 24–31. https://doi.org/10.1016/j.isprsjprs.2016.01.011.

Bey, I., Jacob, D.J., Yantosca, R.M., Logan, J.A., Field, B.D., Fiore, A.M., Li, Q., Liu, H.Y., Mickley, L.J., Schultz, M.G., 2001. Global modeling of tropospheric chemistry with assimilated meteorology: model description and evaluation. J. Geophys. Res. Atmos. 106, 23073–23095. https://doi.org/10.1029/2001JD000807.

Bishop, C.M., 2016. Pattern Recognition and Machine Learning, Information Science and Statistics. Springer, New York.

Bobbink, R., Hicks, K., Galloway, J., Spranger, T., Alkemade, R., Ashmore, M., Bustamante, M., Cinderby, S., Davidson, E., Dentener, F., Emmett, B., Erisman, J.W., Fenn, M., Gilliam, F., Nordin, A., Pardo, L., De Vries, W., 2010. Global assessment of nitrogen deposition effects on terrestrial plant diversity: a synthesis. Ecol. Appl. https://doi.org/10.1890/08-1140.1.

Bowman, W.D., Cleveland, C.C., Halada, Ľ., Hreško, J., Baron, J.S., 2008. Negative impact of nitrogen deposition on soil buffering capacity. Nat. Geosci. 1, 767–770. https://doi.org/10.1038/ngeo339.

Breiman, L., 2001. Random forests. Mach. Learn. 45, 5–32. https://doi.org/10.1023/A:1010933404324.

Brunekreef, B., Holgate, S.T., 2002. Air pollution and health. Lancet. https://doi.org/10.1016/S0140-6736(02)11274-8.

Chang, J.C., Hanna, S.R., 2004. Air quality model performance evaluation. Meteorol. Atmos. Phys. 87, 167–196. https://doi.org/10.1007/S00703-003-0070-7/METRICS.

Clerici, N., Calderón, C.A.V., Posada, J.M., 2017. Fusion of Sentinel-1A and Sentinel-2A data for land cover mapping: a case study in the lower Magdalena region, Colombia. J. Maps 13, 718–726. https://doi.org/10.1080/17445647.2017.1372316.

Colette, A., Aas, W., Banin, L., Braban, C.F., Ferm, M., Ortiz, A.G., Ilyin, I., Mar, K., Pandolfi, M., Putaud, J.-P., Shatalov, V., Solberg, S., Spindler, G., Tarasova, O., Vana, M., Adani, M., Almodovar, P., Berton, E., Bessagnet, B., Bohlin-Nizzetto, P., Boruvkova, J., Breivik, K., Briganti, G., Cappelletti, A., Cuvelier, K., Derwent, R., D'Isidoro, M., Fagerli, H., Funk, C., Vivanco, M.G., Haeuber, R., Hueglin, C., Jenkins, S., Kerr, J., de Leeuw, F., Lynch, J., Manders, A., Mircea, M., Pay, M.T., Pritula, D., Querol, X., Raffort, V., Reiss, I., Roustan, Y., Sauvage, S., Scavo, K., Simpson, D., Smith, R.I., Tang, Y.S., Theobald, M., Torseth, K., Tsyro, S., van Pul, A., Vidic, S., Wallasch, M., Wind, P., 2016. Air Pollution Trends in the EMEP Region between 1990 and 2012. Norwegian Institute for Air Research, Kjeller, Norway.

Cutler, A., Cutler, D.R., Stevens, J.R., 2012. Random forests. Ensemble Mach. Learn 157–175. https://doi.org/10.1007/978-1-4419-9326-7_5.

de Vries, W., Dobbertin, M.H., Solberg, S., van Dobben, H.F., Schaub, M., 2014. Impacts of acid deposition, ozone exposure and weather conditions on forest ecosystems in Europe: an overview. Plant Soil 380, 1–45. https://doi.org/10.1007/s11104-014-2056-2.

de Vries, W., Kros, J., Dolman, M.A., Vellinga, T.V., de Boer, H.C., Gerritsen, A.L., Sonneveld, M.P.W., Bouma, J., 2015. Environmental impacts of innovative dairy farming systems aiming at improved internal nutrient cycling: a multi-scale assessment. Sci. Total Environ. 536, 432–442. https://doi.org/10.1016/j.scitotenv.2015.07.079.

De Vries, W., Leip, A., Reinds, G.J., Kros, J., Lesschen, J.P., Bouwman, A.F., 2011. Comparison of land nitrogen budgets for European agriculture by various modeling approaches. Environ. Pollut. 159, 3254–3268. https://doi.org/10.1016/j.envpol.2011.03.038.

de Vries, W., Schulte-Uebbing, L., Kros, H., Voogd, J.C., Louwagie, G., 2021. Spatially explicit boundaries for agricultural nitrogen inputs in the European Union to meet air and water quality targets. Sci. Total Environ. 786, 147283 https://doi.org/10.1016/J.SCITOTENV.2021.147283.

De Vries, W., Schulte-Uebbing, L., Kros, J., 2020. Assessment of Spatially Explicit Actual, Required and Critical Nitrogen Inputs in EU-27 Agriculture. Wageningen (in press).

Díaz-Uriarte, R., Alvarez de Andrés, S., 2006. Gene selection and classification of microarray data using random forest. BMC Bioinf. 7, 3. https://doi.org/10.1186/1471-2105-7-3.

Dollmann, S., Vermeulen, L., Husman, A.M. de R., 2021. Untangling the governance of public health aspects of manure in The Netherlands. Int. J. Environ. Res. Publ. Health 18. https://doi.org/10.3390/IJERPH182312472.

Drusch, M., Del Bello, U., Carlier, S., Colin, O., Fernandez, V., Gascon, F., Hoersch, B., Isola, C., Laberinti, P., Martimort, P., Meygret, A., Spoto, F., Sy, O., Marchese, F., Bargellini, P., 2012. Sentinel-2: ESA's optical high-resolution mission for GMES operational services. Remote Sens. Environ. 120, 25–36. https://doi.org/10.1016/j.rse.2011.11.026.

Dubovyk, O., Menz, G., Lee, A., Schellberg, J., Thonfeld, F., Khamzina, A., 2015. SPOT-based sub-field level monitoring of vegetation cover dynamics: a case of irrigated croplands. Rem. Sens. 7, 6763–6783. https://doi.org/10.3390/rs70606763.

Elzing, A., Monteny, G.J., 1997. Modeling and experimental determination of ammonia emissions rates from a scale model dairy-cow house. Trans. Am. Soc. Agric. Eng.

Emmons, L.K., Walters, S., Hess, P.G., Lamarque, J.-F., Pfister, G.G., Fillmore, D., Granier, C., Guenther, A., Kinnison, D., Laepple, T., Orlando, J., Tie, X., Tyndall, G., Wiedinmyer, C., Baughcum, S.L., Kloster, S., 2010. Description and evaluation of the model for ozone and related chemical tracers, version 4 (MOZART-4). Geosci. Model Dev 3, 43–67. https://doi.org/10.5194/gmd-3-43-2010.

Erisman, J.W., Bleeker, A., Galloway, J., Sutton, M.S., 2007. Reduced nitrogen in ecology and the environment. Environ. Pollut. https://doi.org/10.1016/j.envpol.2007.06.033.

Erisman, J.W., Sutton, M.A., Galloway, J., Klimont, Z., Winiwarter, W., 2008. How a century of ammonia synthesis changed the world. Nat. Geosci. https://doi.org/10.1038/ngeo325.

Fangmeier, A., Hadwiger-Fangmeier, A., Van der Eerden, L., Jäger, H.J., 1994. Effects of atmospheric ammonia on vegetation-A review. Environ. Pollut. https://doi.org/10.1016/0269-7491(94)90008-6.

Foody, G.M., Pal, M., Rocchini, D., Garzon-Lopez, C.X., Bastin, L., 2016. The sensitivity of mapping methods to reference data quality: training supervised image classifications with imperfect reference data. ISPRS Int. J. Geo-Inf. 5 https://doi.org/10.3390/ijgi5110199.

Fowler, D., Pilegaard, K., Sutton, M.A., Ambus, P., Raivonen, M., Duyzer, J., Simpson, D., Fagerli, H., Fuzzi, S., Schjoerring, J.K., Granier, C., Neftel, A., Isaksen, I.S.A., Laj, P., Maione, M., Monks, P.S., Burkhardt, J., Daemmgen, U., Neirynck, J., Personne, E., Wichink-Kruit, R., Butterbach-Bahl, K., Flechard, C., Tuovinen, J.P., Coyle, M., Gerosa, G., Loubet, B., Altimir, N., Gruenhage, L., Ammann, C., Cieslik, S., Paoletti, E., Mikkelsen, T.N., Ro-Poulsen, H., Cellier, P., Cape, J.N., Horváth, L., Loreto, F., Niinemets, Ü., Palmer, P.I., Rinne, J., Misztal, P., Nemitz, E., Nilsson, D., Pryor, S., Gallagher, M.W., Vesala, T., Skiba, U., Brüggemann, N., Zechmeister-Boltenstern, S., Williams, J., O'Dowd, C., Facchini, M.C., de Leeuw, G., Flossman, A., Chaumerliac, N., Erisman, J.W., 2009. Atmospheric composition change: ecosystems-Atmosphere interactions. Atmos. Environ. https://doi.org/10.1016/j.atmosenv.2009.07.068.

Galloway, J.N., Aber, J.D., Erisman, J.W., Seitzinger, S.P., Howarth, R.W., Cowling, E.B., Cosby, B.J., 2003. The nitrogen cascade. Bioscience 53, 341–356. https://doi.org/10.1641/0006-3568(2003)053[0341:TNC]2.0.CO. ;2.

Ge, X., Schaap, M., Kranenburg, R., Segers, A., Reinds, G.J., Kros, H., de Vries, W., 2020. Modeling atmospheric ammonia using agricultural emissions with improved spatial variability and temporal dynamics. Atmos. Chem. Phys. 20, 16055–16087. https://doi.org/10.5194/acp-20-16055-2020.

Genuer, R., Poggi, J.-M., Tuleau, C., 2008. Random Forests: Some Methodological Insights.

Gies, T.J.A., van, O., Smidt, R.A., Naeff, H., Vos, E., 2015. Geografisch Informatiesysteem Agrarische Bedrijven (GIAB) : Gebruikershandleiding 2010.

Gilliam, F.S., Burns, D.A., Driscoll, C.T., Frey, S.D., Lovett, G.M., Watmough, S.A., 2019. Decreased atmospheric nitrogen deposition in eastern North America: predicted responses of forest ecosystems. Environ. Pollut. 244, 560–574. https://doi.org/10.1016/J.ENVPOL.2018.09.135.

Gislason, P.O., Benediktsson, J.A., Sveinsson, J.R., 2006. Random Forests for land cover classification. Pattern Recogn. Lett. 27, 294–300. https://doi.org/10.1016/j.patrec.2005.08.011.

Goldstein, B.A., Hubbard, A.E., Cutler, A., Barcellos, L.F., 2010. An application of Random Forests to a genome-wide association dataset: methodological considerations & new findings. BMC Genet. 11, 49. https://doi.org/10.1186/1471-2156-11-49.

Griffiths, P., Nendel, C., Hostert, P., 2019. Intra-annual reflectance composites from Sentinel-2 and Landsat for national-scale crop and land cover mapping. Remote Sens. Environ. 220, 135–151. https://doi.org/10.1016/j.rse.2018.10.031.

Guo, Y., Hastie, T., Tibshirani, R., 2007. Regularized linear discriminant analysis and its application in microarrays. Biostatistics 8, 86–100. https://doi.org/10.1093/biostatistics/kxj035.

Gyldenkærne, S., Skjøth, C.A., Hertel, O., Ellermann, T., 2005. A dynamical ammonia emission parameterization for use in air pollution models. J. Geophys. Res. Atmos. 110, 1–14. https://doi.org/10.1029/2004JD005459.

Hafner, S.D., Pacholski, A., Bittman, S., Carozzi, M., Chantigny, M., Génermont, S., Häni, C., Hansen, M.N., Huijsmans, J., Kupper, T., Misselbrook, T., Neftel, A., Nyord, T., Sommer, S.G., 2019. A flexible semi-empirical model for estimating ammonia volatilization from field-applied slurry. Atmos. Environ. 199, 474–484. https://doi.org/10.1016/j.atmosenv.2018.11.034.

Hamaoui-Laguel, L., Meleux, F., Beekmann, M., Bessagnet, B., Génermont, S., Cellier, P., Létinois, L., 2014. Improving ammonia emissions in air quality modelling for France. Atmos. Environ. 92, 584–595. https://doi.org/10.1016/j.atmosenv.2012.08.002.

Hamaoui-Laguel, L., Meleux, F., Beekmann, M., Bessagnet, B., Génermont, S.S., Cellier, P., 2011. Modelling agricultural ammonia emissions : impact on particulate matter formation. In: Conference '"Nitrogen & Global Change : Key Findings - Future Challenges. Edimbourg, United Kingdom.

Hanna, S., Chang, J., 2012. Acceptance criteria for urban dispersion model evaluation. Meteorol. Atmos. Phys. 116, 133–146. https://doi.org/10.1007/S00703-011-0177-1/TABLES/6.

Hao, P., Zhan, Y., Wang, L., Niu, Z., Shakir, M., 2015. Feature selection of time series MODIS data for early crop classification using random forest: a case study in Kansas, USA. Rem. Sens. 7, 5347–5369. https://doi.org/10.3390/rs70505347.

Hendriks, C., Kranenburg, R., Kuenen, J.J.P., Van den Bril, B., Verguts, V., Schaap, M., 2016. Ammonia emission time profiles based on manure transport data improve ammonia modelling across north western Europe. Atmos. Environ. 131, 83–96. https://doi.org/10.1016/j.atmosenv.2016.01.043.

Hutchings, N.J., Reinds, G.J., Leip, A., Wattenbach, M., Bienkowski, J.F., Dalgaard, T., Dragosits, U., Drouet, J.L., Durand, P., Maury, O., De Vries, W., 2012. A model for simulating the timelines of field operations at a European scale for use in complex dynamic models. Biogeosciences 9, 4487–4496. https://doi.org/10.5194/bg-9-4487-2012.

Janitza, S., Hornung, R., 2018. On the overestimation of random forest's out-of-bag error. PLoS One 13, e0201904.

Jiang, J., Stevenson, D.S., Uwizeye, A., Tempio, G., Sutton, M.A., 2021. A climate-dependent global model of ammonia emissions from chicken farming. Biogeosciences 18, 135–158. https://doi.org/10.5194/bg-18-135-2021.

Kavzoglu, T., 2009. Increasing the accuracy of neural network classification using refined training data. Environ. Model. Software 24, 850–858. https://doi.org/10.1016/j.envsoft.2008.11.012.

Kobayashi, N., Tani, H., Wang, X., Sonobe, R., 2020. Crop classification using spectral indices derived from Sentinel-2A imagery. J. Inf. Telecomun. https://doi.org/10.1080/24751839.2019.1694765.

Kros, J., Heuvelink, G.B.M., Reinds, G.J., Lesschen, J.P., Ioannidi, V., De Vries, W., 2012. Uncertainties in model predictions of nitrogen fluxes from agro-ecosystems in Europe. Biogeosciences 9, 4573–4588. https://doi.org/10.5194/bg-9-4573-2012.

Krupa, S.V., 2003. Effects of atmospheric ammonia (NH3) on terrestrial vegetation: a review. Environ. Pollut. https://doi.org/10.1016/S0269-7491(02)00434-7.

Kuenen, J.J.P., Visschedijk, A.J.H., Jozwicka, M., Denier Van Der Gon, H.A.C., 2014. TNO-MACC-II emission inventory; A multi-year (2003-2009) consistent high-resolution European emission inventory for air quality modelling. Atmos. Chem. Phys. 14, 10963–10976. https://doi.org/10.5194/acp-14-10963-2014.

Lan, T., Hu, H., Jiang, C., Yang, G., Zhao, Z., 2020. A comparative study of decision tree, random forest, and convolutional neural network for spread-F identification. Adv. Space Res. 65, 2052–2061. https://doi.org/10.1016/j.asr.2020.01.036.

Li, J., Yang, X., Maffei, C., Tooth, S., Yao, G., 2018. Applying independent component analysis on sentinel-2 imagery to characterize geomorphological responses to an extreme flood event near the non-vegetated Río Colorado terminus, salar de Uyuni, Bolivia. Rem. Sens. 10 https://doi.org/10.3390/rs10050725.

Liu, L., Zhang, X., Xu, W., Liu, X., Li, Y., Lu, X., Zhang, Y., Zhang, W., 2017. Temporal characteristics of atmospheric ammonia and nitrogen dioxide over China based on emission data, satellite observations and atmospheric transport modeling since 1980. Atmos. Chem. Phys. 17, 9365–9378. https://doi.org/10.5194/acp-17-9365-2017.

Lolkema, D.E., Noordijk, H., Stolk, A.P., Hoogerbrugge, R., Van Zanten, M.C., Van Pul, W.A.J., 2015. The measuring ammonia in nature (MAN) network in The Netherlands. Biogeosciences. https://doi.org/10.5194/bg-12-5133-2015.

Louis, J., Charantonis, A., Berthelot, B., Lacoste-Francis, H., 2010. Cloud detection for sentinel-2, living planet symposium. In: EUROPEAN SPACE AGENCY -PUBLICATIONS- ESA SP, Living Planet Symposium. ESA Communications, p. 499. Noordwijk.

Louis, J., Debaecker, V., Pflug, B., Main-Knorn, M., Bieniarz, J., Mueller-Wilm, U., Cadau, E., Gascon, F., 2016. SENTINEL-2 SEN2COR: L2A processor for users. In: Ouwehand, L. (Ed.), Proceedings Living Planet Symposium 2016, ESA Special Publications (on CD), pp. 1–8. Spacebooks Online.

Mack, B., Leinenkugel, P., Kuenzer, C., Dech, S., 2017. A semi-automated approach for the generation of a new land use and land cover product for Germany based on Landsat time-series and Lucas in-situ data. Remote Sens. Lett. 8, 244–253. https://doi.org/10.1080/2150704X.2016.1249299.

Main-Knorn, M., Pflug, B., Louis, J., Debaecker, V., Müller-Wilm, U., Gascon, F., 2017. Sen2Cor for Sentinel-2. https://doi.org/10.1117/12.2278218.

Manders, A.M.M., Builtjes, P.J.H., Curier, L., Gon, H.A.C.D. Vander, Hendriks, C., Jonkers, S., Kranenburg, R., Kuenen, J.J.P., Segers, A.J., Timmermans, R.M.A., Visschedijk, A.J.H., Kruit, R.J.W., Pul, W.A.J.V., Sauter, F.J., Van Der Swaluw, E., Swart, D.P.J., Douros, J., Eskes, H., Van Meijgaard, E., Van Ulft, B., Van Velthoven, P., Banzhaf, S., Mues, A.C., Stern, R., Fu, G., Lu, S., Heemink, A., Van Velzen, N., Schaap, M., 2017. Curriculum vitae of the LOTOS-EUROS (v2.0) chemistry transport model. Geosci. Model. Dev. (GMD). https://doi.org/10.5194/gmd-10-4145-2017.

Manders, A.M.M., Schaap, M., Hoogerbrugge, R., 2009. Testing the capability of the chemistry transport model LOTOS-EUROS to forecast PM10 levels in The Netherlands. Atmos. Environ. 43, 4050–4059. https://doi.org/10.1016/j.atmosenv.2009.05.006.

Marais Sicre, C., Inglada, J., Fieuzal, R., Baup, F., Valero, S., Cros, J., Huc, M., Demarez, V., 2016. Early detection of summer crops using high spatial resolution optical image time series. Rem. Sens. 8 https://doi.org/10.3390/rs8070591.

Menzi, H., Pain, B., Sommer, S.G., 2002. Manure management: the European perspective. In: Ong, H.K., et al. (Eds.), Proc. 4th Int. Livestock Waste Management Symp. and Technology Expo, Penang, Malaysia, ISBN 983-99519-2-0, pp. 35–44.

Mercier, A., Betbeder, J., Rumiano, F., Baudry, J., Gond, V., Blanc, L., Bourgoin, C., Cornu, G., Ciudad, C., Marchamalo, M., Poccard-Chapuis, R., Hubert-Moy, L., 2019. Evaluation of sentinel-1 and 2 time series for land cover classification of forest–agriculture mosaics in temperate and tropical landscapes. Rem. Sens. 11 https://doi.org/10.3390/rs11080979.

Mestre-Quereda, A., Lopez-Sanchez, J.M., Vicente-Guijalba, F., Jacob, A.W., Engdahl, M. E., 2020. Time-series of sentinel-1 interferometric coherence and backscatter for crop-type mapping. IEEE J. Sel. Top. Appl. Earth Obs. Rem. Sens. 13, 4070–4084. https://doi.org/10.1109/JSTARS.2020.3008096.

Midolo, G., Alkemade, R., Schipper, A.M., Benítez-López, A., Perring, M.P., De Vries, W., 2019. Impacts of nitrogen addition on plant species richness and abundance: a global meta-analysis. Global Ecol. Biogeogr. 28, 398–413. https://doi.org/10.1111/GEB.12856.

Misselbrook, T.H., Van Der Weerden, T.J., Pain, B.F., Jarvis, S.C., Chambers, B.J., Smith, K.A., Phillips, V.R., Demmers, T.G.M., 2000. Ammonia emission factors for UK agriculture. Atmos. Environ. 34, 871–880. https://doi.org/10.1016/S1352-2310(99)00350-7.

Montaghi, A., Larsen, R., Greve, M.H., 2013. Accuracy assessment measures for image segmentation goodness of the Land Parcel Identification System (LPIS) in Denmark. Remote Sens. Lett. 4, 946–955. https://doi.org/10.1080/2150704X.2013.817709.

Móring, A., Vieno, M., Doherty, R.M., Laubach, J., Taghizadeh-Toosi, A., Sutton, M.A., 2016. A process-based model for ammonia emission from urine \hack{\newline} patches, GAG (Generation of Ammonia from Grazing): \hack{\newline}description and sensitivity analysis. Biogeosciences 13, 1837–1861. https://doi.org/10.5194/bg-13-1837-2016.

Nemitz, E., Milford, C., Sutton, M.A., 2001. A two-layer canopy compensation point model for describing bi-directional biosphere-atmosphere exchange of ammonia. Q. J. R. Meteorol. Soc. 127, 815–833. https://doi.org/10.1002/qj.49712757306.

Novelli, A., Aguilar, M.A., Nemmaoui, A., Aguilar, F.J., Tarantino, E., 2016. Performance evaluation of object based greenhouse detection from Sentinel-2 MSI and Landsat 8 OLI data: a case study from Almería (Spain). Int. J. Appl. Earth Obs. Geoinf. 52, 403–411. https://doi.org/10.1016/j.jag.2016.07.011.

Orgiazzi, A., Ballabio, C., Panagos, P., Jones, A., Fernández-Ugalde, O., 2018. LUCAS Soil, the largest expandable soil dataset for Europe: a review. Eur. J. Soil Sci. 69, 140–153. https://doi.org/10.1111/EJSS.12499.

Paulot, F., Jacob, D.J., Pinder, R.W., Bash, J.O., Travis, K., Henze, D.K., 2014. Ammonia emissions in the United States, European Union, and China derived by high-resolution inversion of ammonium wet deposition data: interpretation with a new agricultural emissions inventory (MASAGE_NH3). J. Geophys. Res. Atmos. 119, 4343–4364. https://doi.org/10.1002/2013JD021130.

Pelletier, C., Valero, S., Inglada, J., Champion, N., Dedieu, G., 2016. Assessing the robustness of Random Forests to map land cover with high resolution satellite image time series over large areas. Remote Sens. Environ. 187, 156–168. https://doi.org/10.1016/j.rse.2016.10.010.

Pinder, R.W., Adams, P.J., Pandis, S.N., Gilliland, A.B., 2006. Temporally resolved ammonia emission inventories: current estimates, evaluation tools, and measurement needs. J. Geophys. Res. Atmos. 111, 1–14. https://doi.org/10.1029/2005JD006603.

Pope, C.A., Ezzati, M., Dockery, D.W., 2009. Fine-particulate air pollution and life expectancy in the United States. N. Engl. J. Med. https://doi.org/10.1056/nejmsa0805646.

Radoux, J., Lamarche, C., Van Bogaert, E., Bontemps, S., Brockmann, C., Defourny, P., 2014. Automated training sample extraction for global land cover mapping. Rem. Sens. 6, 3965–3987. https://doi.org/10.3390/rs6053965.

Raymond, J., 2016. Use of Stable Isotopes to Trace the Fate of Applied Nitrogen in Forest Plantations to Evaluate Fertilizer Efficiency and Ecosystem Impacts.

Raymond, J.E., Fox, T.R., Strahm, B.D., Zerpa, J., 2016. Ammonia volatilization following nitrogen fertilization with enhanced efficiency fertilizers and urea in loblolly pine (Pinus taeda L.) plantations of the southern United States. For. Ecol. Manage. 376, 247–255. https://doi.org/10.1016/j.foreco.2016.06.015.

Reiche, J., Verhoeven, R., Verbesselt, J., Hamunyela, E., Wielaard, N., Herold, M., 2018. Characterizing tropical forest cover loss using dense sentinel-1 data and active fire alerts. Rem. Sens. 10 https://doi.org/10.3390/rs10050777.

Riddick, S., Ward, D., Hess, P., Mahowald, N., Massad, R., Holland, E., 2016. Estimate of changes in agricultural terrestrial nitrogen pathways and ammonia emissions from 1850 to present in the\hack{\newline} Community Earth System Model. Biogeosciences 13, 3397–3426. https://doi.org/10.5194/bg-13-3397-2016.

Riddick, S.N., Blackall, T.D., Dragosits, U., Tang, Y.S., Moring, A., Daunt, F., Wanless, S., Hamer, K.C., Sutton, M.A., 2017. High temporal resolution modelling of environmentally-dependent seabird ammonia emissions: description and testing of the GUANO model. Atmos. Environ. 161, 48–60. https://doi.org/10.1016/j.atmosenv.2017.04.020.

Rogers, J., Gunn, S., 2006. Identifying feature relevance using a random forest. Lect. Notes Comput. Sci. (including Subser. Lect. Notes Artif. Intell. Lect. Notes Bioinformatics) 3940 LNCS 173. https://doi.org/10.1007/11752790_12/COVER.–184.

Schaap, M., Banzhaf, S., Scheuschner, T., Geupel, M., Hendriks, C., Kranenburg, R., Nagel, H.-D., Segers, A.J., von Schlutow, A., Wichink Kruit, R., Builtjes, P.J.H., 2017. Atmospheric nitrogen deposition to terrestrial ecosystems across Germany. Biogeosci. Discuss. 1–24 https://doi.org/10.5194/BG-2017-491.

Schaap, M., Timmermans, R.M.A., Roemer, M., Boersen, G.A.C., Builtjes, P.J.H., Sauter, F., Velders, G.J.M., Beck, J.P., 2008. The LOTOS EUROS model: description, validation and latest developments. Int. J. Environ. Pollut. 32, 270. https://doi.org/10.1504/ijep.2008.017106.

Schaap, M., van Loon, M., ten Brink, H.M., Dentener, F.J., Builtjes, P.J.H., 2004. Secondary inorganic aerosol simulations for Europe with special attention to nitrate. Atmos. Chem. Phys. https://doi.org/10.5194/acp-4-857-2004.

Schmitz, A., Sanders, T.G.M., Bolte, A., Bussotti, F., Dirnböck, T., Johnson, J., Peñuelas, J., Pollastrini, M., Prescher, A.K., Sardans, J., Verstraeten, A., de Vries, W., 2019. Responses of forest ecosystems in Europe to decreasing nitrogen deposition. Environ. Pollut. 244, 980–994. https://doi.org/10.1016/J.ENVPOL.2018.09.101.

Skjøth, C.A., Geels, C., 2013. The effect of climate and climate change on ammonia emissions in Europe. Atmos. Chem. Phys. 13, 117–128. https://doi.org/10.5194/acp-13-117-2013.

Skjøth, C.A., Geels, C., Berge, H., Gyldenkaerne, S., Fagerli, H., Ellermann, T., Frohn, L. M., Christensen, J., Hansen, K.M., Hansen, K.M., Hertel, O., 2011. Spatial and temporal variations in ammonia emissions â€" a freely accessible model code for Europe. Atmos. Chem. Phys. 11, 5221–5236. https://doi.org/10.5194/acp-11-5221-2011.

Sommer, S.G., Hutchings, N.J., 2001. Ammonia emission from field applied manure and its reduction—invited paper. Eur. J. Agron. 15, 1–15. https://doi.org/10.1016/S1161-0301(01)00112-5.

Sommer, S.G., Olesen, J.E., Christensen, B.T., 1991. Effects of temperature, wind speed and air humidity on ammonia volatilization from surface applied cattle slurry. J. Agric. Sci. 117, 91–100. https://doi.org/10.1017/S0021859600079016.

Sonobe, R., Yamaya, Y., Tani, H., Wang, X., Kobayashi, N., Mochizuki, K., 2018. Crop classification from Sentinel-2-derived vegetation indices using ensemble learning. J. Appl. Remote Sens. 12, 1–16. https://doi.org/10.1117/1.JRS.12.026019.

Stehman, S.V., 2000. Practical implications of design-based sampling inference for thematic map accuracy assessment. Remote Sens. Environ. 72, 35–45. https://doi.org/10.1016/S0034-4257(99)00090-5.

Stokstad, E., 2019. Nitrogen crisis threatens Dutch environment-and economy. Science 366, 1180–1181. https://doi.org/10.1126/science.366.6470.1180.

Sutton, M.A., Asman, W.A.H., Ellermann, T., Van Jaarsveld, J.A., Acker, K., Aneja, V., Duyzer, J., Horvath, L., Paramonov, S., Mitosinkova, M., Tang, Y.S., Achermann, B., Gauger, T., Bartniki, J., Neftel, A., Erisman, J.W., 2003. Establishing the link between ammonia emission control and measurements of reduced nitrogen concentrations and deposition. Environ. Monit. Assess. https://doi.org/10.1023/A:1021834132138.

Sutton, M.A., Fowler, D., Burkhardt, J.K., Milford, C., 1995. Vegetation atmosphere exchange of ammonia: canopy cycling and the impacts of elevated nitrogen inputs. Water, Air, Soil Pollut. https://doi.org/10.1007/BF01186137.

Sutton, M.A., Reis, S., Riddick, S.N., Dragosits, U., Nemitz, E., Theobald, M.R., Tang, Y.S., Braban, C.F., Vieno, M., Dore, A.J., Mitchell, R.F., Wanless, S., Daunt, F., Fowler, D., Blackall, T.D., Milford, C., Flechard, C.R., Loubet, B., Massad, R., Cellier, P., Personne, E., Coheur, P.F., Clarisse, L., Van Damme, M., Ngadi, Y., Clerbaux, C., Skjøth, C.A., Geels, C., Hertel, O., Wichink Kruit, R.J., Pinder, R.W., Bash, J.O., Walker, J.T., Simpson, D., Horváth, L., Misselbrook, T.H., Bleeker, A., Dentener, F., de Vries, W., 2013. Towards a climate-dependent paradigm of ammonia emission and deposition. Philos. Trans. R. Soc. B Biol. Sci. 368, 20130166 https://doi.org/10.1098/rstb.2013.0166.

Sutton, M.A., Skiba, U.M., van Grinsven, H.J.M., Oenema, O., Watson, C.J., Williams, J., Hellums, D.T., Maas, R., Gyldenkaerne, S., Pathak, H., Winiwarter, W., 2014. Green economy thinking and the control of nitrous oxide emissions. Environ. Dev. https://doi.org/10.1016/j.envdev.2013.10.002.

Vaglio Laurin, G., Belli, C., Bianconi, R., Laranci, P., Papale, D., 2018. Early mapping of industrial tomato in Central and Southern Italy with Sentinel 2, aerial and RapidEye additional data. J. Agric. Sci. 156, 396–407. https://doi.org/10.1017/S0021859618000400.

van der Graaf, S.C., Dammers, E., Schaap, M., Willem Erisman, J., Erisman, J.W., Willem Erisman, J., Erisman, J.W., 2018. Technical note: how are NH3 dry deposition estimates affected by combining the LOTOS-EUROS model with IASI-NH3 satellite observations? Atmos. Chem. Phys. 18, 13173–13196. https://doi.org/10.5194/acp-18-13173-2018.

van der Graaf, S.C., Kranenburg, R., Segers, A.J., Schaap, M., Erisman, J.W., 2020. Satellite-derived leaf area index and roughness length information for surface–atmosphere exchange modelling: a case study for reactive nitrogen deposition in north-western Europe using LOTOS-EUROS v2.0 . Geosci. Model Dev 13, 2451–2474. https://doi.org/10.5194/gmd-13-2451-2020.

van Dobben, H.F., de Vries, W., 2017. The contribution of nitrogen deposition to the eutrophication signal in understorey plant communities of European forests. Ecol. Evol. 7, 214–227. https://doi.org/10.1002/ECE3.2485.

van Os, J., Jeurissen, L.J.J., Naeff, H.S.D., 2016. Geografisch informatiesysteem voor de emissieregistratie van landbouwbedrijven;: GIABplus-bestand 2013 – status A, WOt-technical report. Wettelijke Onderzoekstaken Natuur & Milieu. https://doi.org/10.18174/386756.

van Zanten, M.C., Wichink Kruit, R.J., Hoogerbrugge, R., Van der Swaluw, E., van Pul, W.A.J., 2017. Trends in ammonia measurements in The Netherlands over the period 1993–2014. Atmos. Environ. 148, 352–360. https://doi.org/10.1016/j.atmosenv.2016.11.007.

Velthof, G.L., Oudendag, D., Witzke, H.P., Asman, W.A.H., Klimont, Z., Oenema, O., 2009. Integrated assessment of nitrogen losses from agriculture in EU-27 using MITERRA-EUROPE. J. Environ. Qual. 38, 402. https://doi.org/10.2134/jeq2008.0108.

Velthof, G.L., van Bruggen, C., Groenestein, C.M., de Haan, B.J., Hoogeveen, M.W., Huijsmans, J.F.M., 2012. A model for inventory of ammonia emissions from agriculture in The Netherlands. AtmosEnviron 46, 248–255. https://doi.org/10.1016/j.atmosenv.2011.09.075.

Waldhoff, G., Lussem, U., Bareth, G., 2017. Multi-Data Approach for remote sensing-based regional crop rotation mapping: a case study for the Rur catchment, Germany.

Int. J. Appl. Earth Obs. Geoinf. 61, 55–69. https://doi.org/10.1016/j.jag.2017.04.009.

Werner, M., Ambelas Skjøth, C., Kryza, M., Dore, A.J., 2015. Understanding emissions of ammonia from buildings and the application of fertilizers: an example from Poland. Biogeosciences 12, 3623–3638. https://doi.org/10.5194/bg-12-3623-2015.

Wever, D., Coenen, P., Dröge, R., Geilenkirchen, G.P., 't Hoen, M., Honig, E., WWR, K., Leekstra, A.J., Lagerwerf, L.A., te Molder, R.A.B., Peek, C.J., Smeets, W.L.M., van der Sluis, S.M., Vonk, J., 2019. Informative Inventory Report 2019 : Emissions of Transboundary Air Pollutants in the Netherlands 1990-2017. https://doi.org/10.21945/RIVM-2019-0016.

Wichink Kruit, R.J., Aben, J., de Vries, W., Sauter, F., van der Swaluw, E., van Zanten, M. C., van Pul, W.A.J., 2017. Modelling trends in ammonia in The Netherlands over the period 1990–2014. Atmos. Environ. 154, 20–30. https://doi.org/10.1016/j.atmosenv.2017.01.031.

Wulder, M.A., Hilker, T., White, J.C., Coops, N.C., Masek, J.G., Pflugmacher, D., Crevier, Y., 2015. Virtual constellations for global terrestrial monitoring. Remote Sens. Environ. 170, 62–76. https://doi.org/10.1016/j.rse.2015.09.001.

Yan, S., Yao, X., Zhu, D., Liu, D., Zhang, L., Yu, G., Gao, B., Yang, J., Yun, W., 2021. Large-scale crop mapping from multi-source optical satellite imageries using machine learning with discrete grids. Int. J. Appl. Earth Obs. Geoinf. 103, 102485 https://doi.org/10.1016/j.jag.2021.102485.

Yi, Z., Jia, L., Chen, Q., 2020. Crop classification using multi-temporal sentinel-2 data in the shiyang river basin of China. Rem. Sens. 12 https://doi.org/10.3390/rs12244052.

Zimmermann, J., Fealy, R.M., Lydon, K., Mockler, E.M., O'Brien, P., Packham, I., Smith, G., Green, S., 2016. The Irish Land-Parcels Identification System (LPIS)– Experiences in ongoing and recent environmental research and land cover mapping. Biol. Environ. 116B, 53–62. https://doi.org/10.3318/bioe.2016.04.